2012-09-13

# Exploring the Relationship between Monthly Precipitation and EVI Vegetation Productivity Index of Serengeti Nation Park

Ding, Junyan

UNIVERSITY OF CALGARY

# Exploring the Relationship between Monthly Precipitation and EVI Vegetation Productivity Index of Serengeti Nation Park

by

Junyan Ding

A THESIS

SUBMITTED TO THE FACULTY OF GRADUATE STUDIES

INPARTIAL RULFILMENT OF THE REQUIREMENTS FOR THE

DEGREE OF MASTER OF SCIENCE

DEPARTMENT OF GEOGRAPHY

CALGARY, ALBERTA

AUGUST, 2012

# Table of content

## Figures

## Tables

## Abstract

Precipitation has significant impact on the vegetation productivity in the Serengeti area of eastern Africa, an arid and semi-arid region. Previous studies indicate that the response of vegetation productivity to precipitation varies as the consequence of difference in total precipitation, soil properties, and vegetation type. In order to explore and explain the non-stationary relation between vegetation productivity and each of the mean and the variation of precipitation, I examine the correlation between vegetation and precipitation of Serengeti National Park using monthly precipitation and Moderate Resolution Imaging Spectroradiometer (MODIS) derived Enhanced Vegetation Index (EVI) images from 2001 to 2009. First, I compute the mean EVI and mean precipitation based on monthly images. To separate the mean and variation of precipitation, the mean precipitation is subtracted from each of the original precipitation images; the new series images represent the variation of precipitation. Then the new series of variation of precipitation is subjected to Fourier PCA (principal component analysis) analysis to generate a few (usually five) most representative PCA components. Among the PCA components, PC1 and PC3 are found not correlated with mean precipitation and thus are used together to represent the variation of precipitation of the entire period. To explore the non-stationary relation between EVI and precipitation, geographically weighted regression (GWR) models are used with mean precipitation and PC1 and PC3 as independent variables and mean EVI as dependent variable. Three GWR models are created with 1) mean precipitation alone, 2) PCA components, and 3) both mean precipitation and PCA components together, as independent variables. Finally, global linear least square models are used to detect how the correlations between mean EVI and precipitation are affected by soil WHC (water holding capacity) and N content, and vegetation type (independent variables).

It is found that the highest correlation between mean EVI and mean precipitation occurs at north SNP (Serengeti National Park), and decreases towards both the west and east; the highest correlation between mean EVI and the variation of precipitation occurs in the north SNP and the south-east regions, and decreases towards the north and west. The correlation between mean EVI and both mean and variation of precipitation together are maximized at the west side of north SNP and decrease towards the south-east. The amount of precipitation and soil water holding capacity have a significant impact on the correlations between mean EVI and both mean precipitation and the variation of precipitation; soil nitrogen content has significant impact on the correlation between mean EVI and the variation of precipitation; only forest, woody savanna, and savanna are found to have significant impact on the correlation between mean EVI and the variation of precipitation.

# 1. Introduction

## *1.1 Motivation*

Precipitation has a significant impact on vegetation productivity in arid and semi-arid ecosystems. Numerous studies have been done to understand the impact of precipitation on vegetation activity using the Normalized Difference Vegetation Index (NDVI), a measure of vegetation greenness (Allen et al., 2010; Richard & Poccard, 1998; Scanlon et al., 2002; Li et al., 2004). Those studies either investigated the effect of precipitation on an interannual or seasonal scale (e.g. Nicholson et al., 1990; Camberlin et al., 2007; Martiny et al., 2005) or analyzed the impact of cumulative precipitation during previous months on the vegetation productivity and the lag response time of vegetation (Shinoda, 1995). These studies characterized precipitation and NDVI either by the average over a certain period (e.g. one year or a few months) or by the sum over the period (e.g. Shisanya et al., 2011; Richard & Poccard, 1998). Using the average or the sum we only measure the amount of precipitation but not the characteristics of the variation of precipitation during the period. For example, two regions can receive the same amount of precipitation over the year; but the precipitation can be evenly distributed over the year at one region while more punctuated at another region (e.g. thunder storms). Such differences may result in the difference of total productivity of vegetation between two regions, assuming other conditions are held the same. Runoff is more likely to happen when precipitation is highly variable because rainfall may not be able to infiltrate into the soil in time during intense precipitation. Thus if water is a limited resource, regions that have consistent and continuous precipitation may have higher vegetation productivity than regions that have more variable precipitation.

The temporal variations of precipitation are periodic and affected by different mechanisms that cycle at different time scales such as seasonal variation, the one year cycle and El Niño, a quasi-cyclical phenomenon that occurs with varying intensity every few years, but whose longer-term behaviours is not yet well defined (Black et al., 2003; Karnauskas and Busalacchi, 2009; Janicot et al., 2009; Pohl et al., 2009). The spectrum analysis is a time series analysis method that has been long used in climatology to analyse climatic factors (Yiou et al., 1996). Briefly, this method breaks down original sequential data into different cyclic components which are described by three parameters: magnitude, phase and period/frequency. By this means, spectrum analysis is able to more precisely characterize the whole sequential data by few parameters. Therefore, this method is effective to describe the different aspects of temporal variation of precipitation.

## *1.2 Objective and research questions*

My objective is to separate the amount and temporal variation of precipitation using a time series precipitation raster image and to characterize the temporal variation of precipitation by spectra, and then to use spatial analysis to explore and explain the spatial pattern of the correlation between vegetation productivity and the amount and variation of precipitation in Serengeti, a semi-arid savanna ecosystem in Africa. In this project I will apply spectrum analysis on a nine year period of monthly precipitation and vegetation (satellite image) data to answer two questions:

1. To what extent would the average precipitation and the temporal variation of precipitation be associated with the amount of vegetation productivity over a nine year study period (2001 – 2009)?

2. How do average precipitation, soil water holding capacity, soil nitrogen content and vegetation type affect the relation between precipitation and vegetation productivity identified in the first question?

# 2. Literature Review

The Serengeti National Park is a 14763 $km^2$ conserved savannas ecosystem located at the boundary of Kenya and Tanzania in eastern Africa. In the arid and semi-arid regions, water is the most limited resource and therefore the most important determinant to vegetation structure and growth. The rainfall patterns of equatorial eastern Africa are extremely complex as the result of the large-scale tropical controls, which include several major convergence zones, and which are superimposed upon regional factors associated with lakes, topography and maritime influence (Nicholson, 1996). However, the complexity of the region's rainfall is underlain by rather simple and spatially coherent patterns of temporal variability.

## *2.1 Rainfall climatology of eastern Africa*

The wind and pressure patterns governing the region's climate include three major air streams and three convergence zones (fig. 1). The air streams are Congo air with westerly (blowing from west) and southwesterly (blowing from southewest) flows, the northeast monsoon and the southeast monsoon. Both monsoons, unlike the SW monsoon of Asia, are thermally stable and associated with subsiding air: they are therefore relatively dry. In contrast, the flow from the Congo is humid, convergent and thermally unstable, and therefore associated with

rainfall. These air streams are separated by two surface convergence zones, the Intertropical Convergence Zone (ITCZ) and the Congo Air Boundary; the former separates the two monsoons, the latter, the easterlies (blowing from east) and westerlies. A third convergence zone aloft separates the dry, stable, northerly flow of Saharan origin and the moister southerly flow (Nicholson, 1996).

The climate pattern is described here using months and regions instead of seasons, as "summer" and "winter" occur in Africa at different times in different locations. In July/August, the low pressure over the Sahara lies between the NE trades, or Harmattan, and the humid SW flow. The surface position of the Inter-Tropical Convergence Zone (ITCZ), which separates these two wind systems, lies at about 18° to 20°N. A second convergence zone, the Congo Air Boundary, separates the flows off the Atlantic and Indian Oceans. High pressure prevails over southern Africa at this time. In January, the picture is much reversed, with high pressure over the Sahara and a low over southern Africa. The convergence zones have moved southward, with the ITCZ penetrating far into the southern hemisphere (Nicholson, 2000).

The upper air patterns also shift seasonally. In July/August, the upper-level flow is easterly over most of the continent. Imbedded in the easterlies are three jet streams, the African Easterly Jet (AEJ), the Tropical Easterly Jet (TEJ) and a small easterly maximum at about 10°S. The AEJ and TEJ are important for the development of the July/August rainfall regime over northern Africa. The AEJ, in particular, provides energy for the development and maintenance of rain-bearing disturbances. Over the temperate extremes of the continent, westerlies prevail. Their activities extend further south in January.

The large scale pattern of rainfall and its seasonality at a given location are the direct consequence of these circulation patterns. In the local scale, other factors play a role. Highlands, such as those of the Rift Valley, block the moist, unstable westerly flow of Congo air from reaching eastern coastal areas, especially in Ethiopia and Somalia (fig. 2). More localized leeward rain shadows produce subsiding, dry air. This leads to an extremely complex pattern of rainfall and aridity over the Ethiopian highlands. In addition, the low-level Turkana jet streams produce patterns of descending air which enhance aridity. The cold upwelled water along the Somali coast likewise tends to suppress rainfall. Divergent flow resulting from regional pressure patterns and the extreme heating of the Ethiopian highlands enhance the summer aridity. It is also believed that at least some of the rainfall in East Africa is caused by thermal convection at the local scale.

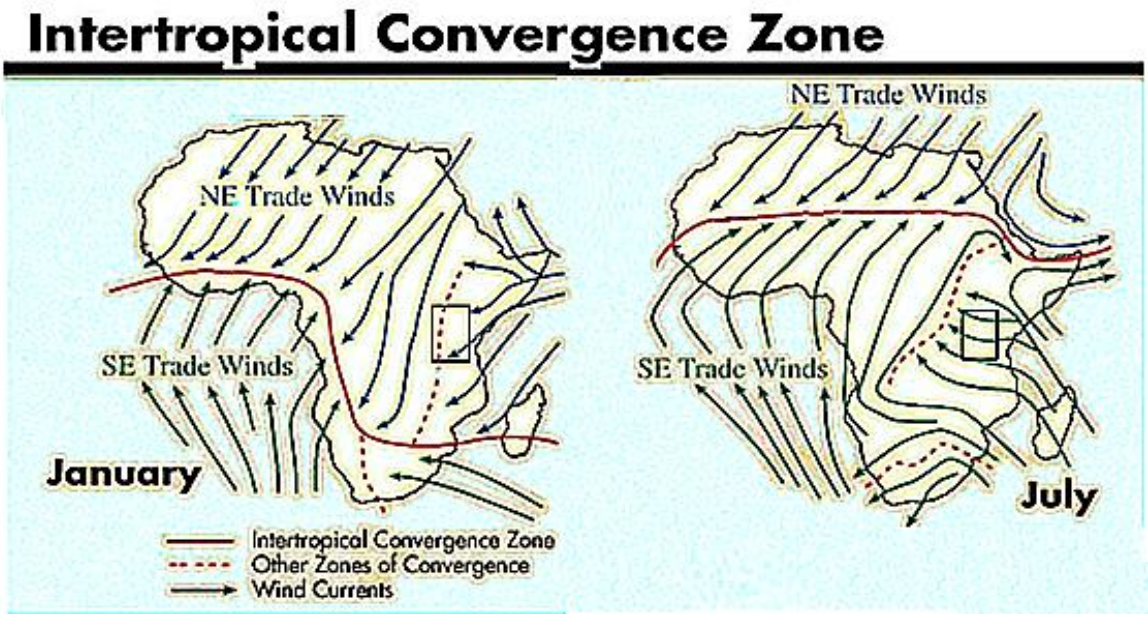


Fig. 1 Schematic of the general patterns of winds and convergence over Africa; solid lines indicate the ITCZ, dashed lines, other convergence zones; black square shows the approximate location of the study area, Serengeti National Park, the vertical red dashed line in top right figure is the Congo Ari Boundary (modified from The Pennsylvania State University, 2011, used by permission)

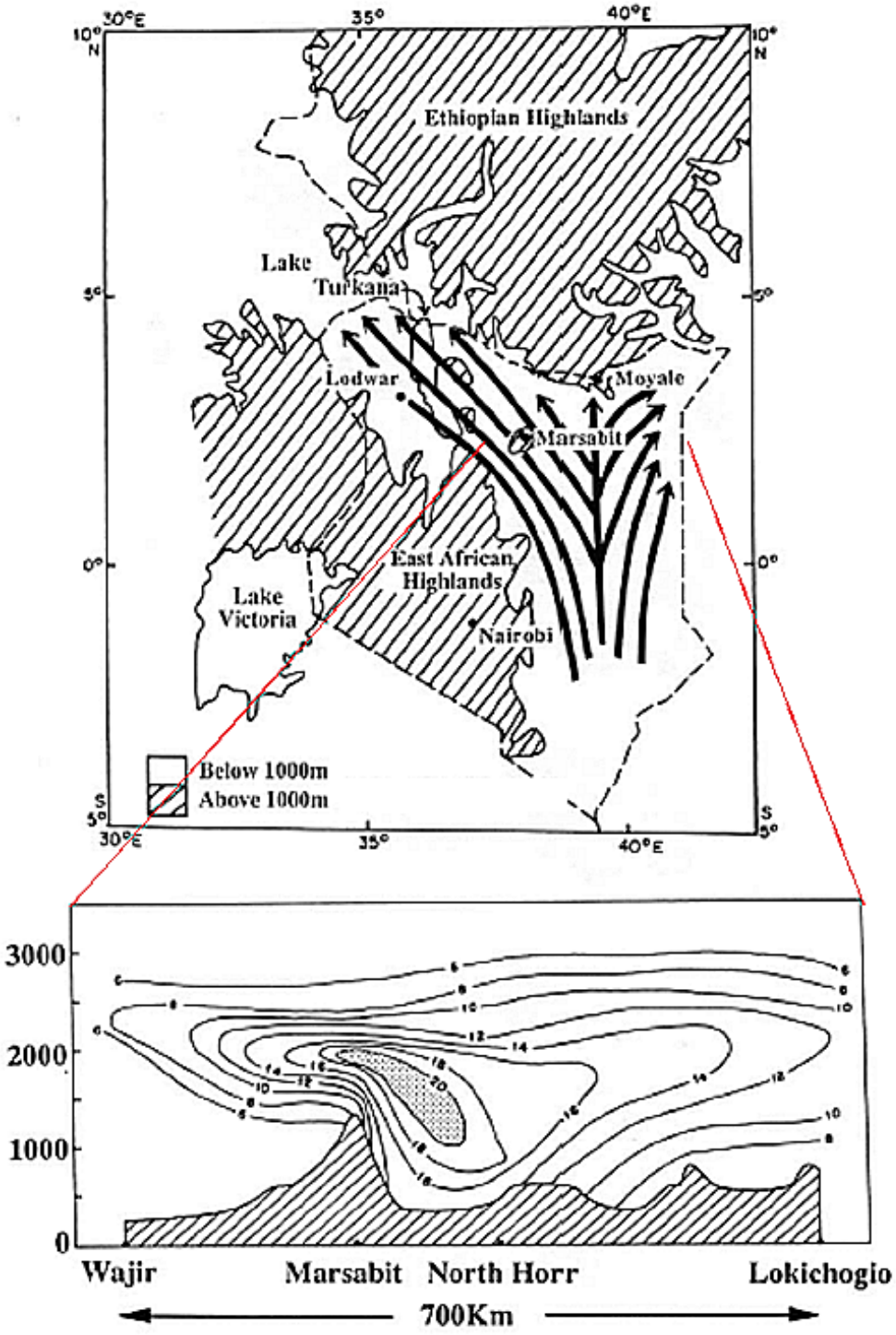


Fig. 2a. Impact of local topography on wind; Small scale topography over eastern Africa and the location of the Turkana jet; b. typical easterly wind speeds of the Turkana jet as a function of altitude (from Nicholson, 1996, used by permission)

As a result of the interaction of the above mechanisms, eastern Africa has great spatial and temporal variability of precipitation. Fig. 3 shows the mean annual precipitation of eastern Africa. The areas with the most rainfall are those with the longest seasons, e.g., the northwest, the areas of highest relief surrounding Mt. Kenya and Mt. Kilimanjaro, and the rugged terrain northeast of Lake Malawi, northwest of Lake Victoria and in Ethiopia. Driest regions are in the northeast, where mean annual rainfall is generally less than 400mm. Rainfall exceeds 800mm in only small portions of Kenya, but exceeds 1200 mm in nearly all of Uganda. Over most of Tanzania, mean annual rainfall is on the order of 800 to 1200 mm (fig. 5).

Much of the region experiences a bimodal seasonal distribution of rainfall, with maxima occurring in the two transition seasons. In large areas of Kenya and a few other regions, there is a third maximum, usually occurring in July or August. In the northern and southern extremes of the regions, the seasonality is unimodal, with the maximum occurring during the high-sun season of the respective hemisphere. The dominant pattern of mean monthly rainfall is a seasonal north-south movement of the main rainbelt, a consequence of the dominant influence of the ITCZ (fig. 4). Heavy rainfall occurs in southern-hemisphere sectors from Dec. to Apr., while intense rains occur from Mar. to May north of the equator and again in Oct. to Nov. From June to Sept. the region is nearly rainless except for an area north and west of Lake Victoria and a small coastal strip from 1 to 7°S. These two areas receive some rainfall nearly year round. However for these areas the only months in which significant rainfall occurs are March and April and, to a lesser extent, November and December. Therefore, the logical climatological seasons are December to March, April to May, June to September and October to November. The four months December to March contribute over 50% of the annual rainfall in the south. In equatorial regions where the seasonal distribution is strongly bi-modal, April-May or sometimes March-May is traditionally

considered to be the “long-rains” while the October-November period is called “short-rains” (Nicholson, 2000).

The ITCZ is the major control of the rainfall in Africa at the regional scale. Its location varies through time as the result of the balance of the strength of SE and NE trade winds that are in turn driven by the gradient of sea surface temperature (SST) of the Atlantic Ocean and the Indian Ocean (fig 6). Three mechanisms act on different time scales to affect the SST. The intra-seasonal variation of the location of ITCZ in Africa is associated with Madden–Julian oscillation (MJO), the intra-annual variation is the result of the asymmetric heating of land and ocean through the year, and the inter-annual variation is affected by Indian Ocean dipole or zone mode (IOZM) and El Niño. El Niños appear every two to seven years (Guilyardi et al., 2009). Recent study shows that the composite ENSO positive episodes result in the positive sea surface temperature (SST) anomalies in the eastern equatorial Atlantic and are accompanied by a southward shift of the ITCZ (Karnauskas and Busalacchi, 2009). The IOZM, identified by Saji et al. (1999) is a less periodic oscillation of sea-surface temperature that occurs with an average of four each positive and negative events during each 30 year period, with each event pair lasting around six months. During negative IOZM years, the “short” rain of eastern Africa is enhanced and during the positive IOZM year, rainfall of Africa is reduced (Black et al., 2003; Saji and Yamagata, 2003; Clark et al., 2003). The MJO is a 30 to 90 day oscillation of SST of the Atlantic Ocean; since it happens in the Atlantic Ocean, studies found it has effects on West Africa monsoons (Janicot et al., 2009; Pohl et al., 2009). Although the causes of these mechanisms have not yet been understood, together they determine the temporal and spatial pattern of rainfall in Eastern Africa as described above.

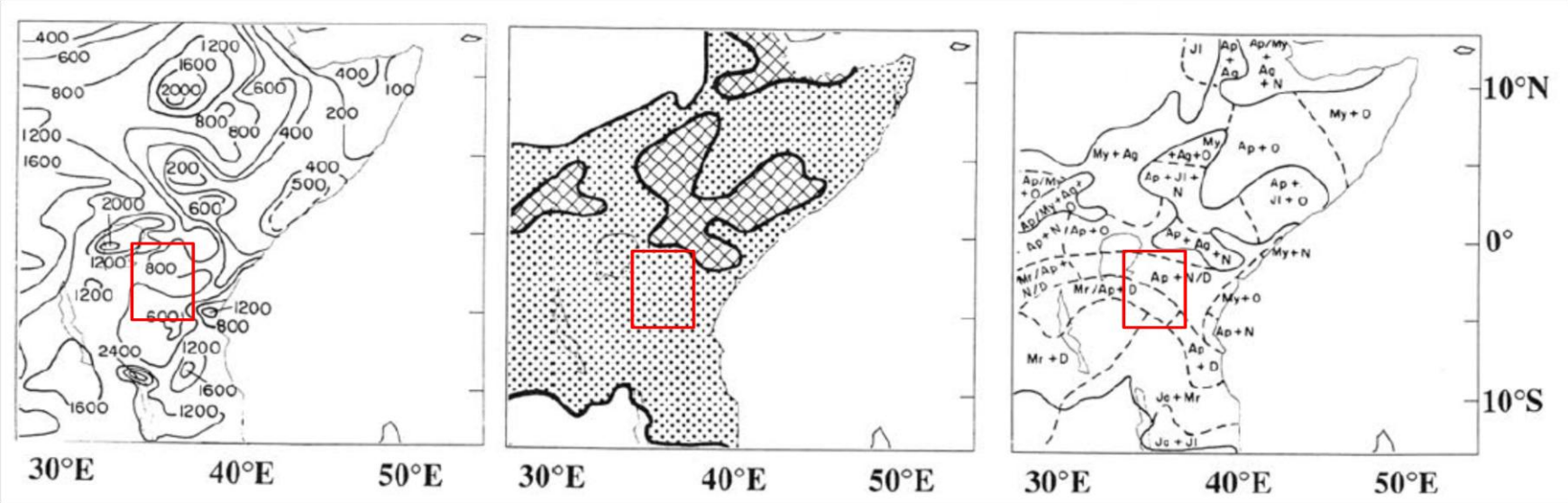


Fig. 3a Map of rainfall characteristics over East Africa (from Nicholson, 1996, used by permission). Top left: mean annual rainfall; Top right: distribution of unimodal (no-shading), bimodal (dots), and trimodal (hatching) rainy seasons; Bottom: months of peak rainfall; red rectangle represents the location of study area;


3b. reference map of East Africa ( from Free World Maps, 2012)

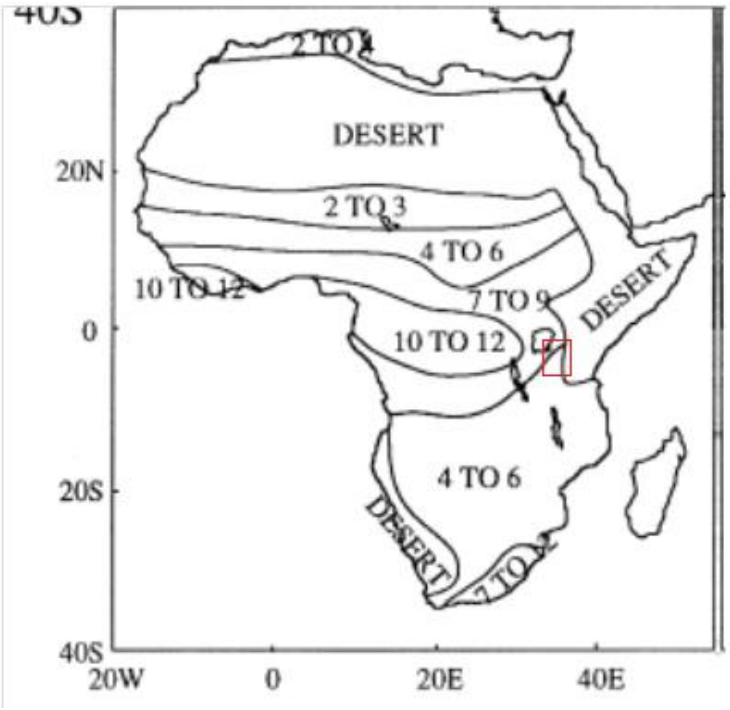


Fig. 4 Length of the rainy season by months (from Nicholson, 2000, used by permission): SNP is indicated by red square

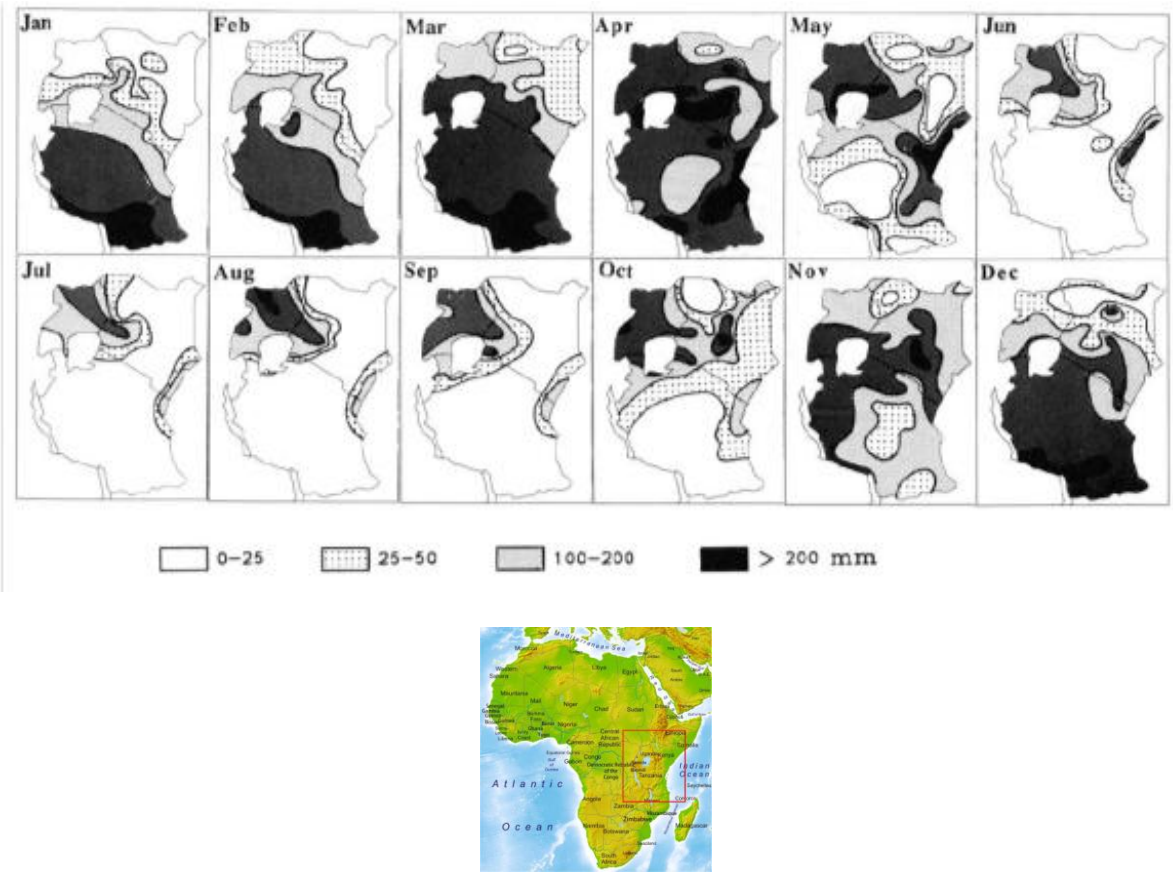


Fig. 5 Mean monthly rainfall of East Africa (from Nicholson, 1996, used by permission): the red square in the small Africa map represents the location of the study area

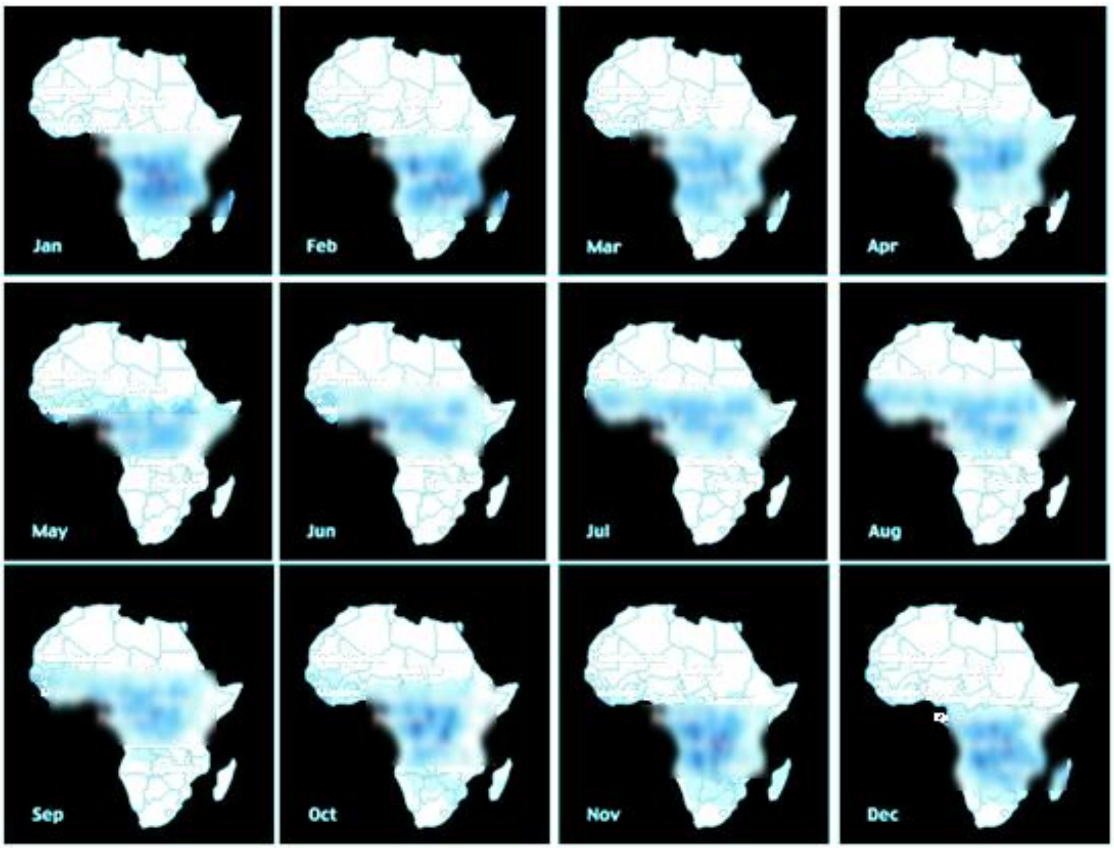


Fig. 6. Average monthly cloud cover (blue region) which indicates the location of ITCZ of Africa (from University of South Carolina, 2011, used by permission)

## 2.2 impact of rainfall on productivity in eastern Africa

The Normalized Difference Vegetation Index (NDVI) is generally recognized as a good indicator of terrestrial vegetation productivity (Wang et al., 2003). Previous studies of the relationship between precipitation and NDVI in Africa were focused on the inter-annual variation of rainfall. It was found that the pattern of vegetation activity was strongly related to rainfall in areas with between 200 – 600 mm annual precipitation, the so called semi-arid area (Davenport and Nicholson, 1993; Nicholson et al., 1990; Camberlin et al, 2007). Within this rainfall range, the correlation between mean annual rainfall and a vegetation index (VI) can be well described by a linear regression (Martiny et al., 2005). However, the slopes of these

regression lines are different at different locations due to differences in vegetation types. The marginal response of annual NDVI to an increase or a decrease in annual rainfall is maximized at this rainfall range (Camberlin et al, 2007). The previous year's rainfall also has an impact on current year NDVI, particularly in the year following either a drought or a particularly wet year (Martiny et al., 2005); a drought year has negative impact on the following year's NDVI and a wet year has positive impact on next year's NDVI. In addition, soil properties including available water capacity, organic matter and pH have an impact on the relationship between annual rainfall and NDVI in semi-arid areas. Above 1000mm annual precipitation, these factors do not have significant impact (Camberlin et al, 2007). Maximum local NDVI is associated with some of the largest rainfalls in semi-arid regions and with some lowest rainfalls in mesic regions (Chamaillé-Jammes and Fritz, 2009).

The lag of NDVI increase after rainfall was found to change with the season. The seasonal correlation of rainfall and NDVI is significant between 200 – 600mm annual precipitation. A linear relationship is found for seasonal variations in semi-arid areas; above 800 – 1000 mm annual precipitation, NDVI tends to be saturated (Martiny et al., 2006). During the long rain (April – May), the lag is 1 to 2 months, while during the short rain (Nov. – Dec.) the lag time is 2 to 3 months. The rate that NDVI increases with precipitation during rainy seasons is higher in the long rain (0.03) and low in the short rain (0.02). Another study found the best correlation is found to be between the current month's NDVI and the average rainfall of three previous months (Davenport and Nicholson, 1993). Using a linear regression, the best correlation between rainfall and NDVI is found during the short rain season ($R = 0.83$), and it is lowest but still considerable during the long rain season ($R = 0.76$) (Martiny et al., 2010).

Nicholson et al. (1990) studied the impact of vegetation on the relationship between annual rainfall and NDVI. They found in forest regions there is little relationship between total NDVI and rainfall; also little year-to-year variation of NDVI even when rainfall varies significantly. Highest NDVI values are attained for the driest forest. In woodlands, it was found there is less month-to-month variation; the period of minimum NDVI is longer and more pronounced than in the forest. Although mean annual rainfall is from 634 – 1009 mm, dry month minimum NDVI is close to 0.1. In bushland/thicket areas, NDVI fluctuation closely corresponds to rainfall fluctuation in both timing and magnitude. They also found that the map of the ratio of annual NDVI to annual rainfall resembles the vegetation map of tropical Africa. This finding indicates vegetation has impact on NDVI – rainfall relationship.

The above discussion indicates that vegetation productivity in Africa changes with precipitation. However, due to the difference in total precipitation, vegetation type, and soil properties, vegetation productivity changes with precipitation in different ways. As studies show the precipitation in Africa has cyclic properties, we can expect that vegetation productivity in Africa also has cyclic properties but as impacted by other factors vegetation productivity may have different cycles from precipitation.

## *2.3 Time series analysis*

### 2.3.1 Time series data and two analysis approaches

Time series data are regularly spaced sequences of observations which are ordered in time, such as hourly, daily, monthly observations of precipitation, temperature, or productivity, etc. There are two basic approaches to time series analysis: time-domain analysis and frequency-domain analysis. Time-domain methods seek to characterize data series in the same terms in

which they are observed and reported (Wilks, 1995). This approach tends to identify the mechanism of how the current stage is affected by a previous stage, in other words the correlation between two time-adjacent stages. Frequency-domain analysis represents data series in terms of contributions occurring at different time scales, or characteristic frequencies (Wilks, 1995). Each time scale is represented by a pair of sine and cosine functions (Ghil et al., 2002). The overall time series is the linear combination of this collection of sine and cosine waves oscillating at different rates, each corresponding to a time scale.

### 2.3.3 Analysis of time series by frequency domain

The frequency domain approach is motivated by the observation that the most regular, and hence predictable, behaviour of a time series is to be periodic. This approach then proceeds to determine the periodic components embedded in the time series by computing the associated periods, amplitudes, and phases, for each component wave (Ghil et al., 2002). By this means, the frequency domain approach provides insight into the dynamics of the underlying system that generated the series.

#### *2.3.3.1 Harmonic Analysis*

Harmonic analysis consists of representing the fluctuations or variations in a time series as the linear combination of a series of sine and cosine functions at different time scales. A simple time series having a sinusoidal character and executing a single cycle can be described using the following equation (Wilks, 2002):

$$y_t = \bar{y} + C_1 \cos\left(\frac{2\pi t}{n} - \emptyset_1\right) \quad (1)$$

$$= \bar{y} + \left(a_1 \cos\frac{2\pi t}{n} + b_1 \sin\frac{2\pi t}{n}\right)$$

Where $y_t$ is the original time series data, $\bar{y}$ is the shifting of the cosine function to the general level of the data, $C_1$ is the amplitude, n is the total number of the observation, $2\pi/n$ is the period of the cosine function, $Ø_1$ is the phase representing the shifting of the cosine function to the right. The second equation uses trigonometric functions to expand this equation to another format. Fig. 7 describes the transformation of a formal cosine function.

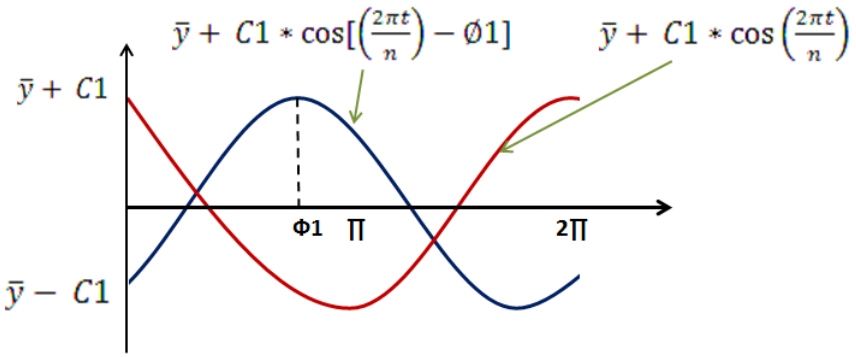


Fig. 7 Transformation of a simple cosine function defined on 0 to 2π radians to a function representing a data series on the interval 0 to n time units

Any data series consisting of n points can be represented exactly, meaning that a harmonic function can be found that passes through each of the points, by adding together a series of n/2 harmonic functions (Wilks, 1995),

$$y_t = \bar{y} + \sum_{k=1}^{n/2} \{C_k \cos(\frac{2\pi kt}{n} - Ø_k)\} \quad (2)$$

$$= \bar{y} + \sum_{n=1}^{k} \left(a_k \cos\frac{2\pi kt}{n} + b_k \sin\frac{2\pi kt}{n}\right)$$

The cosine wave comprising the k=1 term of the equation is the fundamental, or first harmonic, that was the subject of the previous section. The other n/2 -1 terms in the summation of the equation are higher harmonics, or cosine waves with frequencies $GƆ_k = 2\pi k/n$, that are integer multiples of the fundamental frequency. Figure 8 shows a linear combination of the two cosine curves.

Practically, a single harmonic wave will represent most time series very well; just as adding more predictors to a multiple regression will improve the fit to a set of dependent data, with each successive addition adding less new information, adding more cosine waves to a harmonic analysis will improve the fit to any real time series. However, many real phenomenon such as climatic factors, though show periodic variation, do not vary in a perfect sine/cosine form. This is the disadvantage of the Fourier transform.

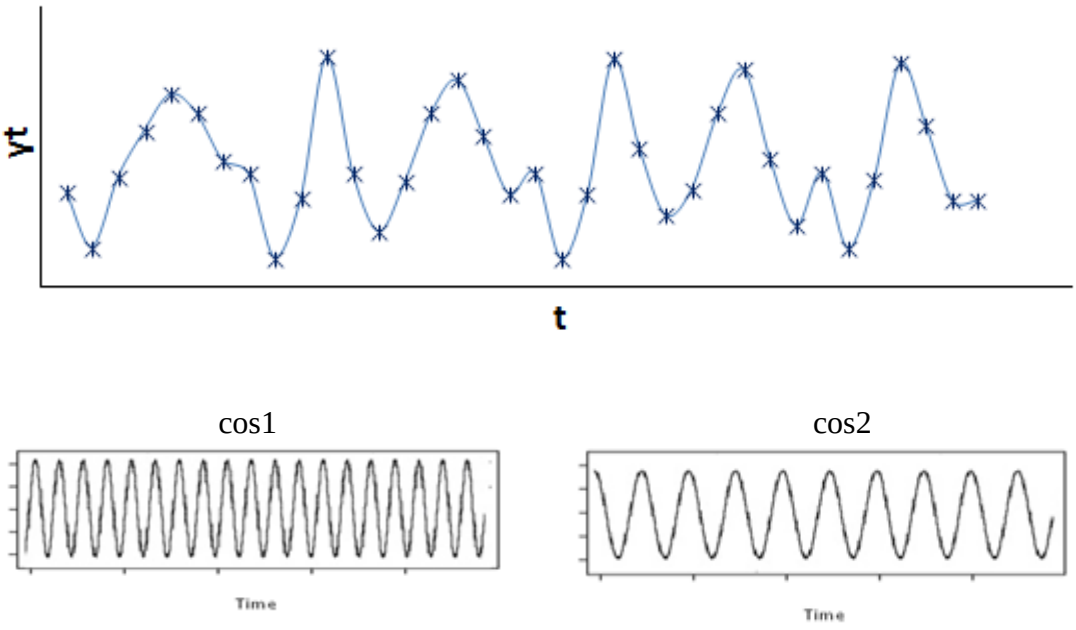


Fig. 8 Linear combination of two cosine curves; y=2*cos1+3*cos2

### *2.3.3.2 Spectral Analysis*

Instead of looking at a time series as a collection of data points $y_t$ measured as a function of time, spectral analysis looks at the time series as a collection of Fourier coefficients, magnitude $C_k$ and phase $Ø_k$, as a function of frequency $ƠƟ_k$, which is examined using the periodogram, also called a power spectrum. The vertical axis is the proportion of the amplitude at the plotted frequency to the sum of the squared amplitudes $C_k^2$. The periodogram I at frequency f =j/n is defined to be:

$$I\left(\frac{j}{n}\right) = \frac{n}{2}\left(A_j^2 + B_j^2\right) \qquad (3)$$

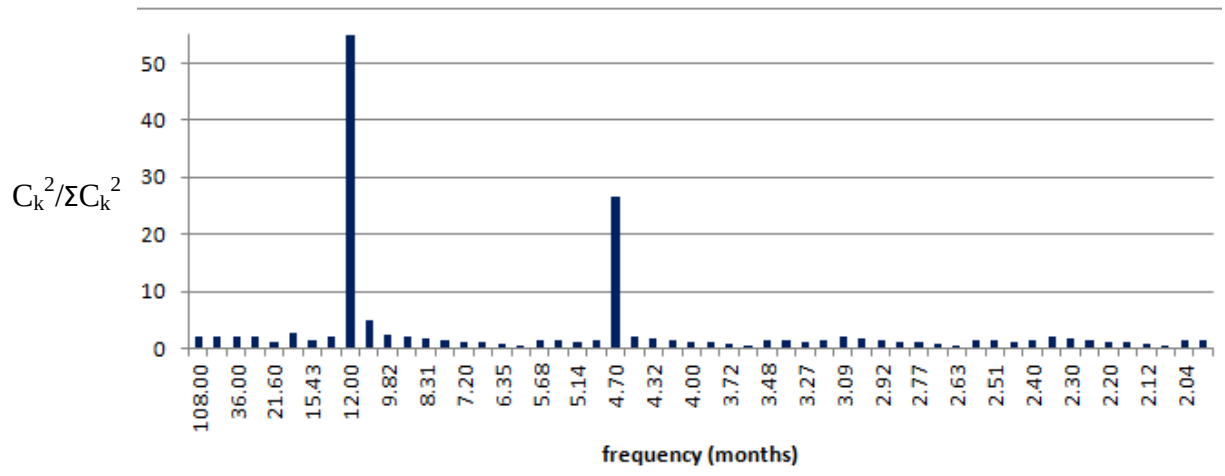


Fig. 9 Periodogram of the series in fig. 8 (from Cryer and Chan, 2008, used by permission)

A relatively large value of *I*(*j*/*n*) indicates relatively more importance for the frequency *j*/*n* (or near *j*/*n*) in explaining the oscillation in the observed series. *I*(*j*/*n*) is proportional to the squared correlation between the observed series and a cosine wave with frequency *j*/*n*. The dominant frequencies might be used to fit cosine (or sine) waves to the data, or might be used simply to describe the important periodicities in the series. The phases represent when each cycle

peaks. Since a phase exists and can be mapped for each pixel, the phases of different cycles can be used in mapping the spatial variation of the time that each component is maximized.

## *2.4 Geographically Weighted Regression (GWR)*

Stationary simply means constant, or 'still' over entire duration in time or region in space. "Spatial nonstationarity is a condition in which a simple 'global" model cannot explain the relationships between some sets of variables" (Brunsdon et al., 1996). In other words, there is non-constant relationship between a dependent variable and explanatory variables. Geographically weighted regression (GWR) is a recent technique aimed to catch the spatial non-stationarities. In my project I use GWR to describe the non-stationary relation between precipitation and vegetation productivity in Serengeti National Park, East Africa. In order to appropriately use this technique, I review the technique background of GWR, the criticisms to GWR and its application in the relevant studies previously.

### 2.4.1 Theoretical background of GWR

GWR is a local model designed to deal with the issue of spatial non-stationary processes. GWR computes the linear model in the same way as the ordinary least square model (OLS), the standardized linear regression model which also know as global model in contrast to local model. The difference is that instead of generating one linear relation for the entire region, GWR constructs separate equations for every feature, a geographical entity represents an real world object such as a forest or a political district, in the dataset incorporating the dependent and independent variables of features nearby, and the impact of neighbors is weighted by the distance of the neighbor to that feature. The GWR function can be written as (Griffith, 2008):

$$Y = \beta_0(u,v) + \sum_{p=1}^{p} \mathrm{X_p}\beta_\mathrm{p}\ (\mathrm{u,v}) + \ \varepsilon \qquad (4)$$

where *Y* is an n x 1 vector of dependent variable, $\beta_0$ is the intercept, $\beta p$ is the *p*th regression coefficient, *Xp* is an n x 1 vector of values of the independent variable *p*, ε is a vector of errors, and (u, v) is the geocoded coordinates of a location. The regression coefficients are being weighted. The estimation of the coefficients is based on weighted least squares theory; the parameter estimates for a linear regression model weighted by distance are (Griffith, 2008):

$$\widehat{\beta}\ (u,v) = [X^T W(u,v) X]^{-1} X^T W(u,v) Y \qquad (5)$$

where W(u, v) is a diagonal matrix whose wjj (u, v) entries define the geographic field for each location *i*. The weight is set in the way that the observations nearby a given location, where the parameter estimates are to be computed, have more influence on estimation than observations farther away. Among many different kernel functions (weight schemes), the two most commonly used are the Gaussian function (equation 6) and the bi-square function (equation7) (Fotheringham et al., 2002):

$$w_{ij}(u,v) = exp(\frac{-d_{ij}}{h})^2 \qquad (6)$$

$$w_{ij}(u,v) = (1 - \left(\frac{-d_{ij}}{h}\right)^2)^2 \qquad (7)$$

where *dij* is the Euclidean distance separating the location of observation *i* , whose coordinates are (u, v), and location of observation *j*, and *h* is the `bandwidth'. Bandwidth can be selected by cross validation (CV) or Akaike information criterion (AIC). Minimizing the AIC provides a trade-off between goodness-of-fit and the degrees of freedom (DF) or model reliability, as a decrease in DF reduces the model reliability.

### 2.4.2 Issues of GWR

Though GWR provides a solution to deal with spatial non-stationary issues, it is a relatively new technique and has some problems. Currently, there are three major issues of GWR: 1. problems caused by multicollinearity; 2. impact of spatial autocorrelation; and 3. impact of parameter setting (patterns of induced spatial heterogeneity as a result of the spatial weighting of the observations in each local regression).

"Evaluating data in GWR for local multicollinearities and pairwise correlations between sets of local coefficients is even more important than in the traditional global regression model due to the increased complexities of the GWR estimation procedure that potentially induces interrelationships among the local estimates" (Wheeler and Tiefelsdorf, 2005). However, commonly used the tools such as bivariate correlation and scatter plot only identify multicollinearity on the global scale. Multicollinearity of independent variables in GWR can cause the correlation between corresponding coefficients and generates an induced spatial pattern which does not actually exist (Wheeler and Tiefelsdorf, 2005; Wheeler, 2006; Wheeler and Calder, 2007; Griffith, 2008). Another problem of multicollinearity of independent variables is the unreliable estimation of the regression coefficients, of which the side effect could be a tendency for GWR to overestimate how much the regression coefficients vary in space (O'Sullivan and Unwin, 2010).

Spatial non-stationary is the non-constant variation of a variable or a relationship over the space while spatial autocorrelation measures the similarity or difference of a variable in terms of spatial proximity of locations. GWR is designed to detect spatial non-stationarity but not spatial autocorrelation. In reality, both spatial non-stationary and spatial autocorrelation processes exist at the same time. As stated by the first law of geography, adjacent things are more related than

distant things (Tobler, 2004). There will be high local correlation in both dependent variable and independent variables. GWR is a local model, thus is more susceptible to the problem of spatial autocorrelation. The local correlation of dependent variables can significantly reduce the degree of freedom, and the result is the local overfitting of the model – very high local $R^2$ at some locations where the dependent variable has high local spatial correlation (Cho et al., 2010), and highly unreliable estimation of coefficients (O'Sullivan and Unwin, 2010).

Furthermore, GWR outcomes are affected by the setting of parameters, especially the bandwidth. For example, Wheeler and Tiefelsdorf, (2005) found that decreasing bandwidth increased the effect of multicollinearity, and there is an optimal kernel size above which multicollinearity is not longer a problem. Farber and Páez (2007) found that the goodness-of-fit (local $R^2$) is maximized when bandwidths are small, and decreases as bandwidths increase. Thus, when using adaptive bandwidth selection method, the spatial heterogeneity of local $R^2$ may be an artifact of the variation of bandwidth. Furthermore, the optimal bandwidth can vary too. First, the weight, w(ui,vi), can be computed using different kernel functions such as the triangular or Bartlett kernel, Epanechnikov kernel, bisquare kernel, and tricube kernel; and the bandwidth changes with the type of kernel function (Cho et al., 2010). Second, when using cross calibration, the optimal bandwidth is also affected by extreme values. (Farber and Páez, 2007). In addition, there is a relationship between coefficient heterogeneity and bandwidth size as the variance-bias trade off (Fotheringham et al., 2002). Coefficient variability increases as bandwidth decreases; the problem is that smaller bandwidths, which typically produce tighter fitting predictions, exhibit higher levels of coefficient variability and are plagued with extreme coefficients perhaps as a result of over-fitting (Farber and Páez, 2007). Therefore, even though estimation accuracy is

maximized at smaller bandwidths, when the focus of analysis is exploratory, not predictive, the primarily concern is the reliability of the spatial distributions of estimated parameters.

### 2.4.3 Application of GWR in relevant studies

The issues of GWR discussed above are mainly about the GWR's reliability for making predictions. However, GWR was originally developed to explore the spatial non-stationarities as denoted by the title of one of the first papers of GWR: "A method for exploring spatial nonstationarity" (Brunsdon et al., 1996). Thus these issues become less important if GWR is used as an exploratory method, which is what I am doing in this project.

GWR has been used in different ecosystems and regions to explore the spatial non-stationary relations between vegetation productivity and environmental factors. In two similar studies recently conducted in China, GWR was used to describe the spatial variation of the relation between NDVI and altitude, temperature, precipitation, and topography of an ecosystem and a semiarid mountain watershed (Wang et al., 2005; Zhao et al., 2010). The outcome of GWR was compared with the ordinary least square (OLS) model by the AIC value, goodness of fit and residuals; GWR was found to make significant improvement over OLS. Zhao et al. (2010) further found that the effect of topographic and climatic factors on vegetation is weak in regions with small spatial variations in LAI.

Some studies found that the spatial patterns of the response of vegetation productivity to precipitation as mapped intercept, slope, and goodness of fit appear to correspond with some patterns in vegetation and topographic position (Propastin and Kappas, 2008; Nippert et al., 2011). Propastin and Kappas (2008) found that the value of local $R^2$ tends to display the highest values in the area where steppe vegetation dominates (local $R^2 = 0.92$ to 0.96), and the lowest in the regions of desert vegetation. Desert vegetation correlates lower with the patterns of rainfall

(local $R^2$ = 0.70 to 0.92). Nippert et al. (2011) used GWR to explore the impact of topography on the vegetation productivity in the Great Plains grassland in North America, and found that the plant growth is low in upland areas and increases towards lowland areas.

Furthermore, Propastin (2012) modified GWR by incorporating elevation into a GWR model to deal with both horizontal and vertical non-stationarities to provide better estimation of aboveground biomass from remote sensing images in the mountain rainforest ecosystem in Central Sulavesi, Indonesia.

One thing worth mentioning is that all these studies had compared the outcomes of GWR with field studies or other studies on the same region; and the outcomes of GWR appeared to be consistent with other studies. These studies demonstrate that with all the issues (for example the variation of local $R^2$s in Propastin and Kappas (2008) could be the result of spatial autocorrelation), GWR is still a valid technique in exploring the non-stationary relation between climatic factors and vegetation productivity of different ecosystems and in different places.

### 2.4.4 MODIS EVI

Plants have evolved to absorb solar radiation in the photosynthetically active radiation (PAR) spectral region (400 nm – 700 nm), which is used in the process of photosynthesis. Plants also reflect solar radiation in the near-infrared spectral (NIR) region. Consequently, healthy green plants appear dark (low reflection, high absorption) in the PAR and bright (high reflection) in the NIR. By contrast, non-vegetated surfaces tend to have relatively higher reflectance in the PAR region and lower or equal reflectance in the NIR region. Based on this mechanism, the normalized difference vegetation index (NDVI), calculated as (NIR – R)/ (NIR + R), has been developed to yield a single value to be used to assess vegetation status (Rouse et al., 1973). By correlating space-derived NDVI values with ground-measured values, NDVI has been used to

estimate a large number of vegetation properties such as leaf area index (LAI), biomass, gross primary productifvity (GPP), net primary productivity (NPP), and fractional vegetation cover (Lillesand and Kiefer, 2006). For example, MODIS has global GPP and NPP products which are generated by incorporate NDVI and daily temperature (Zhao et al., 2005).

However NDVI is affected by a number of factors. It tends to become saturated (i.e. does not increase with addition of more leaves) in a highly productive ecosystem such as tropical rain forest. NDVI is also affected by atmospheric conditions such as moisture content and aerosols, which may change reflection in wavelength-selective ways. Furthermore, the background soil, particularly the moisture content of the soil, has an impact on NDVI values. To reduce the impact of atmospheric properties, Kaufman and Tanere (1992) proposed a modification to NDVI, ARVI (atmospherically resistant vegetation index) calculated as: (NIR- (R – γ (B-R)))/(NIR+ (R – γ (B-R))), where R is the reflectance in the red band, B is the reflectance in the blue band, and γ is a constant whose value depends on the aerosol characteristics of atmosphere. To minimize the effect of soil background, Huete (1988) incorporated a constant L into the original NDVI formula. The new index is called SAVI (soil-adjusted vegetation index) and is calculated as: (NIR-R (1+L)) / (NIR+R+L), where R is the reflectance in the red band; the value of L is 0.0 for low vegetation cover and 1.0 for complete vegetation cover.

Another new vegetation index, the Enhanced Vegetation Index (EVI), was developed by Huete et al. (2002), which combined the advantages of ARVI and SAVI. EVI was developed to optimize the vegetation signal with improved sensitivity in high biomass regions and improved vegetation monitoring through a de-coupling of the canopy background signal and a reduction in atmosphere influences (Heute et al., 2002):

$$EVI = G\,\frac{N - R}{N + C_1 R - C_2 B + L}$$

where N, R, and B are atmospherically corrected or partially atmosphere- corrected (Rayleigh and ozone absorption) surface reflectances in near-infrared, red and blue bands respectively; G is a gain factor; C1, C2 are the coefficients of the aerosol resistance term, which uses the blue band to correct for aerosol influences in the red band, and L functions as the soil-adjustment factor. EVI not only gains its heritage from SAVI and ARVI, but also improves the linearity with vegetation biophysical parameters, encompassing a broader range in LAI retrievals (Houborg et al., 2007). These modified indices require the availability of a blue band, which was not present on all sensors. Since the launch of MODIS in 1999, the blue band has been available. Thus, EVI is tied to the Moderate Resolution Imaging Spectroradiometer (MODIS) sensor aboard the NASA Terra satellite. MODIS has 36 spectral bands ranging in wavelength from 0.4 µm to 14.4 µm and at varying spatial resolutions (250 m to1 km) (NASA, 2012). Together MODIS captures the images of the entire Earth every 1 to 2 days. MODIS also has three on-board calibrators (a solar diffuser combined with a solar diffuser stability monitor, a spectral radiometric calibration assembly, and a blackbody) which provide in-flight calibration. These are all required to calculate the coefficients of EVI. Therefore, EVI cannot be computed effectively without the whole MODIS system. The coefficients adopted in the MODIS EVI algorithm are L=1, C1=6, C2=7.5, and G=2.5 (Huete et al., 2002). MODIS was launched in Dec. 1999. The earliest images available for downloading were taken in March 2000. Thus in order to take advantage of EVI, my study period is limited to 2001 to 2009 as the precipitation data are only available till 2009. The MODIS EVI series continues beyond 2009.

MODIS has global composite EVI products from 2001 in both 16 days and month time scale. The 16 day composite EVI is produced by first selecting the high quality pixels (cloud-free, nadir view pixel with no residual atmospheric contamination) from the 64 images over the entire 16 day period, and then the maximum EVI among the filtered pixels, which best represents the condition, is used to set a single value for each pixel; then the monthly composite EVI is produced based on 16-day composite EVI by applying a weighting factor based on the degree of temporal overlap to each in put (Solano et al., 2010). By this means, the composite monthly EVI is not an image of a particular day of a month but a best representative of the entire month. MODIS derived EVI was found to correlate well with estimated gross primary productivity on a site-by-site basis across the whole of Africa (Sjöström et al., 2011). Thus, the composite EVI is chosen as a surrogate for GPP that is independent to temperature in this project.

# 3. Methods

## *3.1 study area*

The Serengeti ecosystem (Fig. 10), an area of about 25,000 $km^2$ on the border of Tanzania and Kenya, east Africa ($34^0$ to $36^0$ E, $1^0$ to $3^0$ 30' S), is functionally defined by the seasonal migration of 1.2 million wildebeest and is comprised of Serengeti National Park and a string of game reserve areas which buffer the core protected area from areas of unrestricted land use and intense human settlement. The ecosystem itself is defined by two major habitat types, short grass plains and savanna woodlands. There is great spatial heterogeneity. The southeastern plains are treeless except along Olduvai Gorge. The grasses are alkaline-tolerant. The woodlands start at a sharp boundary running south of Seronera in one direction and east of Seronera in the other. The woodlands are dominated by Acacia species in all area except for a small region south and west

of Kogatende, where the Terminalia-Combretum forest type takes over. Tree cover varies between 2% and 30%. Along the main rivers, Mbalageti, Grumeti, and Mara and its tributaries, there is a gallery forest with a closed canopy (Sinclair, 1995).

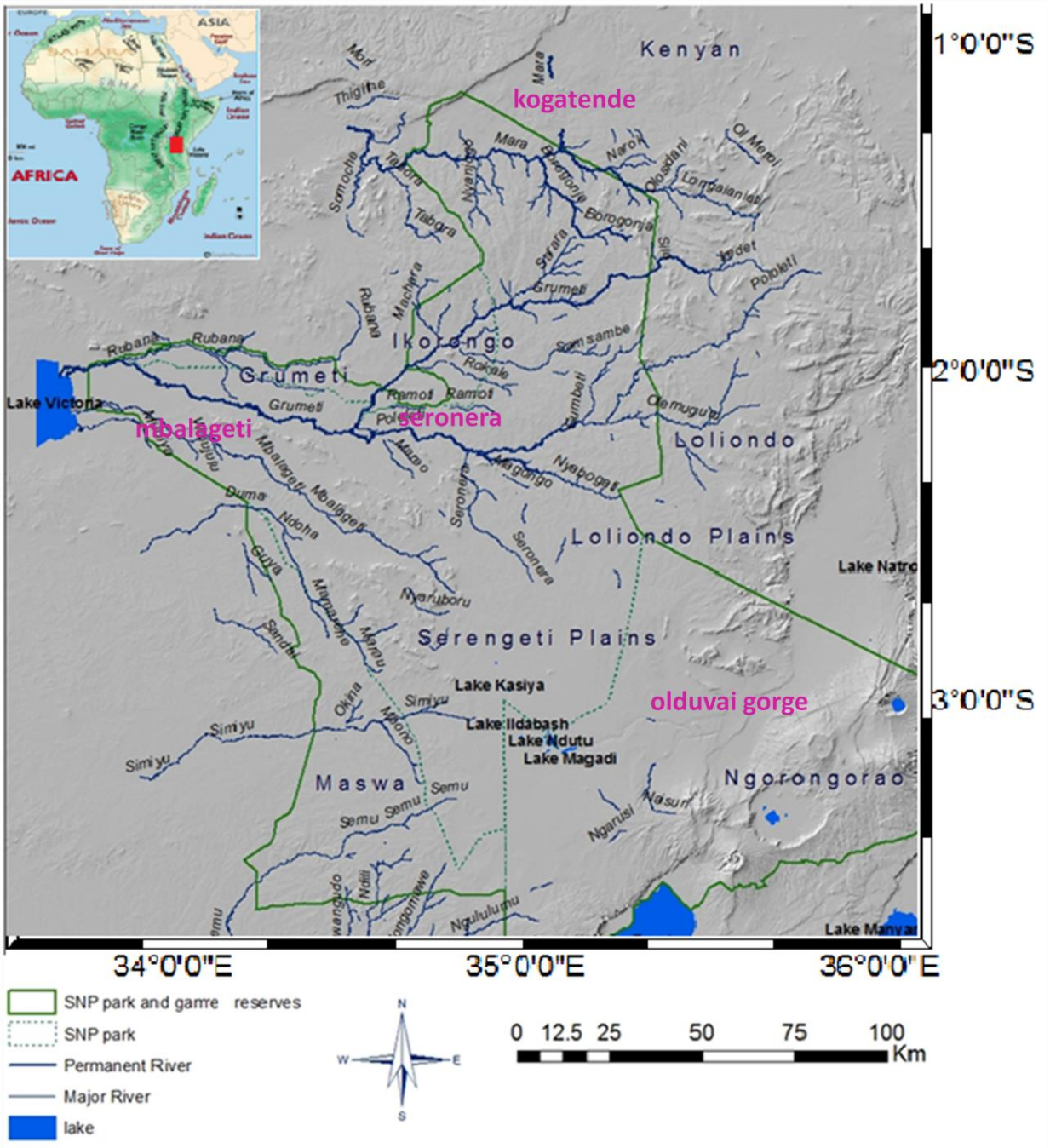


Fig. 10 The Serengeti ecosystem and its major landscape features

The climate of the Serengeti ecosystem is both varied and varying; varied, because the precipitation ranges from true grasslands (<550 mm mean annual precipitation) in the southeast to broadleaf miombo woodlands in the northern extension (precip <900mm) over a relatively short distance (200 km) (Map 1). Spatially, landform influences the local weather system by producing a rainfall gradient via two landscape features: the Crater highlands and Meru-Kilimanjaro mountain range to the east, and Lake Victoria to the west. Prevailing winds from the east carry moisture originating from the Indian Ocean and release it in the form of precipitation as they cross the highlands thus producing a rain shadow to the west of the mountains. In contrast, winds originating from the west carry moisture eastwards from Lake Victoria, counteracting this rain shadow effect from the east, leading to the rainfall gradient. Precipitation is also varying because the broader-area climate exhibits temporal variability, particularly with regard to rainfall. Inter-annual rainfall variability in East Africa, an effect of the El Niño/Southern Oscillation (ENSO), is one of the more important controlling factors (Janowiak, 1988; Ropelewski and Halpert, 1987; 1989; 1996). The SNP is located at the intersection of the regional climatic controls that interact with the local and regional topographic and water body effects.

The Serengeti is part of the high interior plateau of East Africa. It slopes from its highest part (1850m) on the eastern plains near the Gol Mountains toward Speke Gulf (920 m). West of a line going through Seronera, the underlying geology consists of very old Precambrian (2500 ma) volcanic rock and banded ironstone. Soils on the eastern plains are highly saline and alkaline, and are also shallow as a result of their recent volcanic origins. The soils become progressively deeper and less alkaline toward the northwestern plains and into the woodlands. The soil catena, which is the gradient of soil types from ridge top to drainage sump, is characterized by shallow,

sandy, well-drained soil at the top, changing to deep, silty, poorly drained soil at the bottom (Sinclair, 1995).

## *3.2 Data*

### 3.2.1 Precipitation map

Rainfall data in Serengeti National Park have been collected by the Serengeti Ecological Monitoring Programme, the Serengeti National Park ecologist, Serengeti Wildlife Research Institute, and Tanzania Wildlife Conservation Monitoring, and made available by NREL (2011). There are 40-50 rain gauges in and around the park (Figure 11) which are read each month during the last few days of the month. The gauges are thick pipes closed at one end and buried in the ground. There are many instances where a rain gauge was only read after 2 or 3 months, thus the amount in the gauge was the cumulative total over the period. A computer program was developed to distribute the cumulative amount among the months for which there were no readings (Coughenour, 1992). The program searched for the nearest gauge with data for all months, and the proportional distribution of rainfall among months at that gauge was used to distribute the cumulative amount among months at the gauge with missing readings.

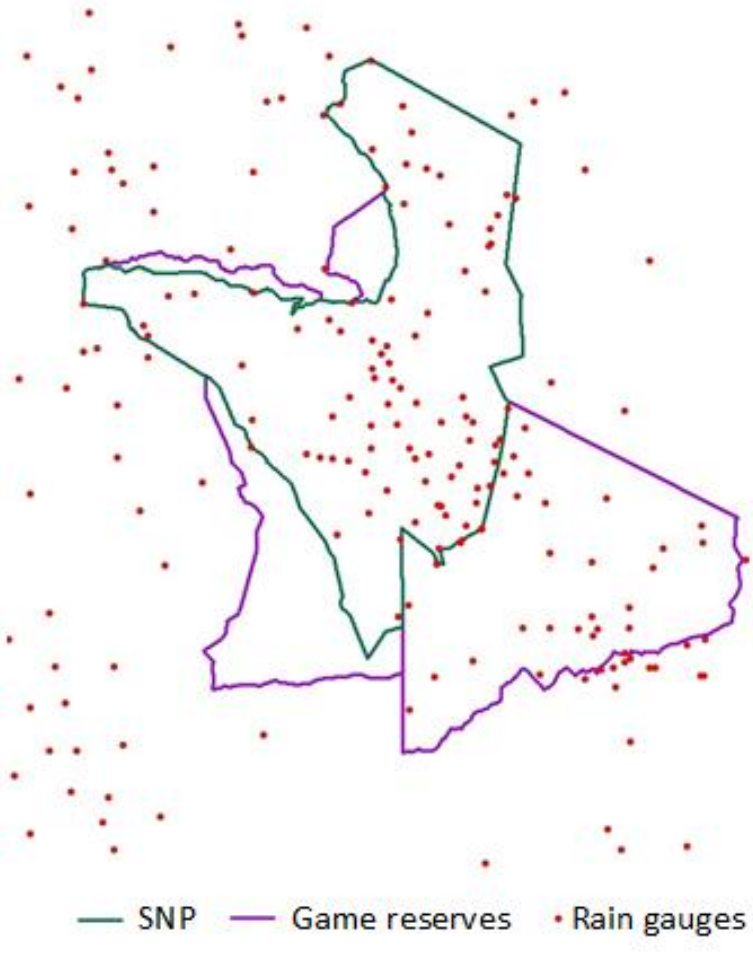


Fig. 11 location of rain gauges

Monthly rainfall maps from 2001 to 2009 were produced for the Greater Serengeti using a program called PPTMAP, developed by Coughenour (1992). This was used to interpolate the rainfall data, accounting for significant elevation effects. The model is based on an algorithm to spatially interpolate point data, while correcting for effects of elevation. The program has both Gaussian and Inverse Distance weighting algorithms. The Inverse Distance weighting has the advantage of creating rainfall maps where the mapped value nearly exactly matches the observed value at each data point. This is because the weight, the inverse of distance to a power, takes on extremely high values close to a station, and essentially an infinite value at the station. This

approach works very well with high quality data sets that have sufficient station densities and few or minimal recording errors. However, if there are insufficient station densities relative to actual spatial variation, and when there are suspected recording errors, Inverse Distance weighting produces rainfall maps that show noticeable rings or "bulls-eyes" resulting from radially decreasing distance weights farther away from each station. In contrast, the Gaussian weighting approach does not force the estimates to exactly match the observed data. Instead, the estimate at any point is the outcome of all surrounding data points weighted by a distance function that resembles half of a normal (Gaussian) distribution. This approach essentially averages out discrepancies among stations that might arise from recording errors, and bulls-eye artefacts are eliminated. The Gaussian approach was used here, with the alpha parameter set to 6.25, as in Thornton et al. (1997). The 10 closest stations were included in the estimate for each point. Including too many stations was found to produce excessive smoothing over the region, unrealistically reducing local highs and increasing local lows.

PPTMAP corrects for elevation differences between the location of the point in question and the rain gauge locations before carrying out the interpolation. The principle is that higher elevation results in cooler temperatures within a given air mass. Cooler temperatures are closer to the dew point, resulting in greater precipitation for a higher point, when precipitation results from a single large weather system. It is not an effective correction for very small local convection-induced storms. For each rain gauge with data, a regression between rainfall and elevation is carried out using data from gauges within a specified distance range, here 75 km. The significance of the regression is assessed using the F-test, with at $P<0.1$. The program searches for outlier data points in the regression using the Z statistic. Here, a point was considered an outlier if the Z statistic was greater than 2.0 or less than -2.0. The outliers are

discarded and the regression is recalculated. The slopes of significant regressions for each gauge are then used in the distance weighting calculation. Thus, when a distance weighted estimate is calculated, the actual data point for each gauge is first corrected for the elevation difference using the slope of the regression line (increase in rainfall per meter of elevation gain) before it is weighted by the Gaussian distance function. All maps were produced on a 1 km grid.

### 3.2.2 MODIS data

The monthly composite MODIS EVIs (MOD 13A3) in 1km resolution from 2001 to 2009 were downloaded from the Global Land Cover Facility (GLCF) website (http://glcf.umd.edu/data/modis/index.shtml, Oct. 2011), to match precipitation data which are obtained by month. The vegetation of the park is characterised by MODIS land cover type (MOD12Q1).

### 3.2.3 Soil map

The soil map developed by FAO is used to produce the maps of water holding capacity and nitrogen content. The map of soil water holding capacity of the soil great group and nitrogen content of the study area are extracted from the Digital Soil Map of the World version 3.5 (FAO, 1995).

## *3.3Statistical analysis*

### 3.3.1 Impact of average precipitation and its temporal variation on average EVI

The analysis is based on MODIS 1km x 1 km pixels, which means the smallest spatial unit is one pixel. For precipitation, I compute the mean precipitation of the entire period, and then extract the mean precipitation from each original layer. The resulting data layer series shows the variation of precipitation of the entire period. To create a periodogram for the variation of

precipitation, sub-waves with different periods are extracted using Fourier transformation through decomposing the original monthly precipitation from 2001 to 2009. The frequency of sub-waves ranges from 1 wave over the entire period to n/2 complete waves over the series (n is the total number of layers). The results are a series of layers, one per wave, representing the magnitude of each wave. These layers together form the periodograms of precipitation. Literally, the independent variable of the periodogram is the proportion of the square of the magnitude of a given frequency to the sum of the squared magnitude of all frequencies – in other words, the portion of the total dataset magnitude (for each pixel) that is represented by this period. However, in this project I will use magnitude as the independent variable directly instead of using the proportion. This is because I am not only interested in identifying the dominant frequency but also in the spatial pattern of the magnitudes of different cycles across the region. Magnitude itself is comparable from one pixel to another; the proportion is not. Thus here the periodogram of the series spatial data will be composed of 54 raster layers with each layer representing the magnitude of one frequency. I will also compute the averages of precipitation and EVI of the entire nine year period.

The periodogram of precipitation represents the temporal variation of precipitation. It is impractical to visually examine all the series of periodograms of precipitation and hope to extract a meaningful idea of the relationships among the various pixels. Therefore we need to reduce the data to simpler representations. To do that, I apply Principal Component Analysis (PCA) on these raster layers. PCA is a method used to look for recurring patterns of variability. The outcome of PCA is PCA components (images, also called eigenchannels) and loadings. The digital numbers of the images are the scales and the values of loadings are correlations measuring how well each component is correlated with original image series. The first PCA

components that explain the majority of the variance (about 80%) are used together to represent the temporal variation of precipitation instead of all 54 input layers. These PCA components are tested for multicollinearity with mean precipitation. The ones that are found not correlated with mean precipitation and are thus used together to represent the variation of precipitation of the entire period. Then mean precipitation and the selected PCA components are used as independent variables in regression models with mean EVI as the dependent variable.

In order to detect the existing of the non-stationary relationship between precipitation and mean EVI, a global model is created first using all the mean precipitation and selected PCA components. If the diagnostic statistic of the global model indicates that the non-stationary relationship exists, then three GWR models are created with independent variables 1) mean precipitation alone, 2) PCA components and 3) both mean precipitation and PCA components together. The inputs of GWR are rescaled to 5km resolution from the original 1 km resolution images (by averaging the area) for two reasons. First, the current GWR softwares only allow 1000 records, which can be satisfied with 5km images. Second, as previous studies show the topography affects on EVI only in small area, in this study I am not able to incorporate topography into the model. Thus I reduce the effect of topography by aggregating the data. The adaptive bandwidth selection method calibrated using AIC is used in GWR with the Gaussian function. The spatial variation of the corresponding local $R^2$s indicate how well mean EVI is correlated with mean precipitation alone, temporal variation of precipitation alone, and with both mean and temporal variation of precipitation together. Finally, global linear least square models are used to detect how the correlations between mean EVI and precipitation are affected by mean precipitation, soil WHC and N content, and vegetation type. The independent variables of OLS models are mean precipitation, soil WHC and N content, and vegetation type (vegetation type is

treated as dummy variable). The local $R^2$s of three GWR models are used as dependent variable of the OLS models. Figure 12 is the flow chart of data analysis.

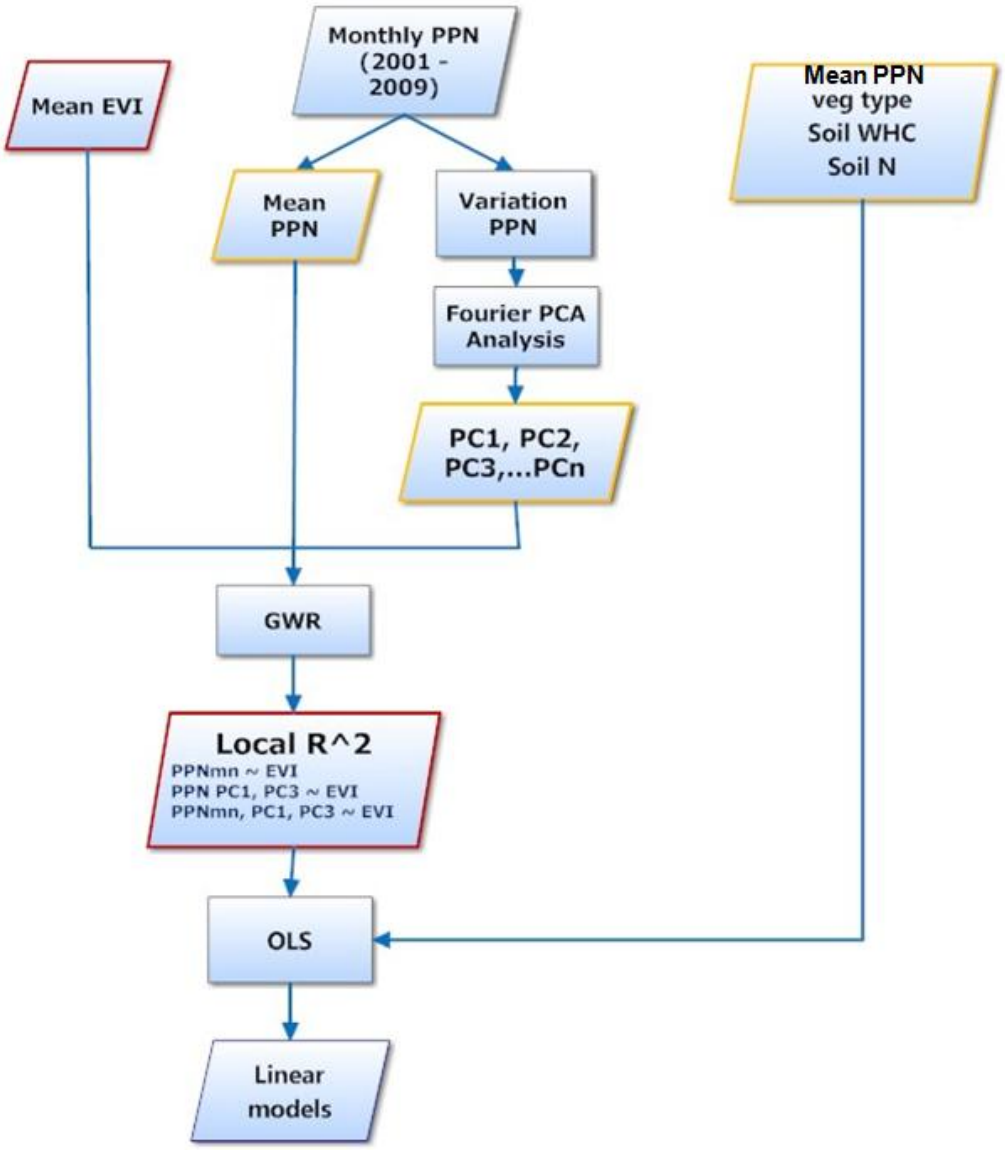


Fig. 12 Data analysis

PPN: mean precipitation ; GWR: geographically weighted regression; PCA : principal component analysis; OLS: Linear, ordinary least squares model

# 4. Results

## *4.1 Outcome of spectrum analysis on precipitation variation*

The outcomes of Fourier transformation are 54 images as the magnitude of different cycles with period range from 108 month to 2 month. Figure 14 shows the spectrum of 17 selected locations/pixels (figure 13b) which are believed to best represent a variety of the spectrums over the entire study area. To choose the l7 location, I first arbitrarily selected 54 pixels (figure 13a) cover the entire study area; then run a cross correlation test, the closely located pixels (about ten neighbor pixels) with highly correlated spectrum (Pearson's r >0.75) are removed in order to reduce the repeated pattern of spectrum while still cover the entire study area.

The spectrums of selected 17 pixels differ in certain ways. First, most of the pixels have a clear dominance of annual (12 month) cycle over other cycles except pixel 3 and 4. Among those annual cycle dominated pixels, some pixels show especially high magnitude of annual cycle over other cycles (pixel 6, 7, 8, 9, 12, 13, 14, 15, 16, 17), while some pixels only show a slightly higher magnitude of annual cycle ( pixel 1, 2, 5, 10, 11). Second, some pixels have high magnitude of most cycles (pixel 3, 4, 5, 10) but some have relative low overall magnitudes (pixel 7, 13, 14, 15, 16), and for the rest pixels, the magnitudes of different cycles vary. In addition, pixel 12 and 17 seem to have slightly higher magnitudes of larger cycles (period is larger than one year) than those small cycles. By comparing the PC1 values between these pixels, it appears that high PC1 values tend to be mainly associated with the dominance of annual cycle over other cycles. The large PC1 value represents less dominant of annual cycle and small PC1 value indicates strong dominance of annual cycle. From the image, it appears that the north-west corner has the highest PC1 value. This region is close to the lake Victoria. Precipitation there is

more affected by local geographical feature, the lake, than ITCZ. Thus this region has relative constant precipitation over time. When moving away from the lake, precipitation is more affected by ITCZ. There is no obvious pattern for PC3. PC3 shows small scale variation thus is more likely to be associated with topographical effects.

## *4.2 Selecting PCA outcomes of precipitation*

The PCA on the magnitude of the cycles generated by Fourier transform generates 20 components. The percentage of the total variation explains by each PCA component is shown in table 2 and figure 13. First three PCA components, PC1, PC2, and PC3 together explain 74% of the total variance of the magnitude of all the cycles. Then there is a fast drop in the percentage variance explained by later PCA components. PC4 explains 7% of the variance and does not contain specific bright or dark spots within the study area. Though including PC4 can catch 80% of the variance, I decided not to include PC4. This is because the more explanatory variables used in the regression model, the less reliable the model is. Since statistics and regression models are used extensively in this project; they already bring in uncertainties. Therefore, I chose PC1, PC2, and PC3 (figure 14) together to represent the entire temporal variation of precipitation. The loadings of PC1, PC2, and PC3 (figure 15) show that PC1 has about-equal positive loading of the majority cycles thus explains the most of the variance in the cycles in the same direction. The exceptions are cycles 2.6, 4.9, 6, 12, 21.6, and 108 month cycles. PC2 catches contrast between the strongly positively loaded and negatively loaded cycles. PC3 has highly negative loading of long term cycles and tend to have fluctuate loadings of short cycles, thus tend to catches the most

variation of long term cycles. The correlation between the mean precipitation and each of PC1, PC2 and PC3 measured by Pearson's r, are 0.363, 0.759, and -0.415 respectively. Thus using 0.7 as the critical value, mean precipitation and PC2 are correlated. Thus PC1 and PC3 are used together to represent the temporal variation of precipitation.

Fig. 13 a. locations of original randomly selected pixels; b. the location of final 17 pixels. the background image is the PC1

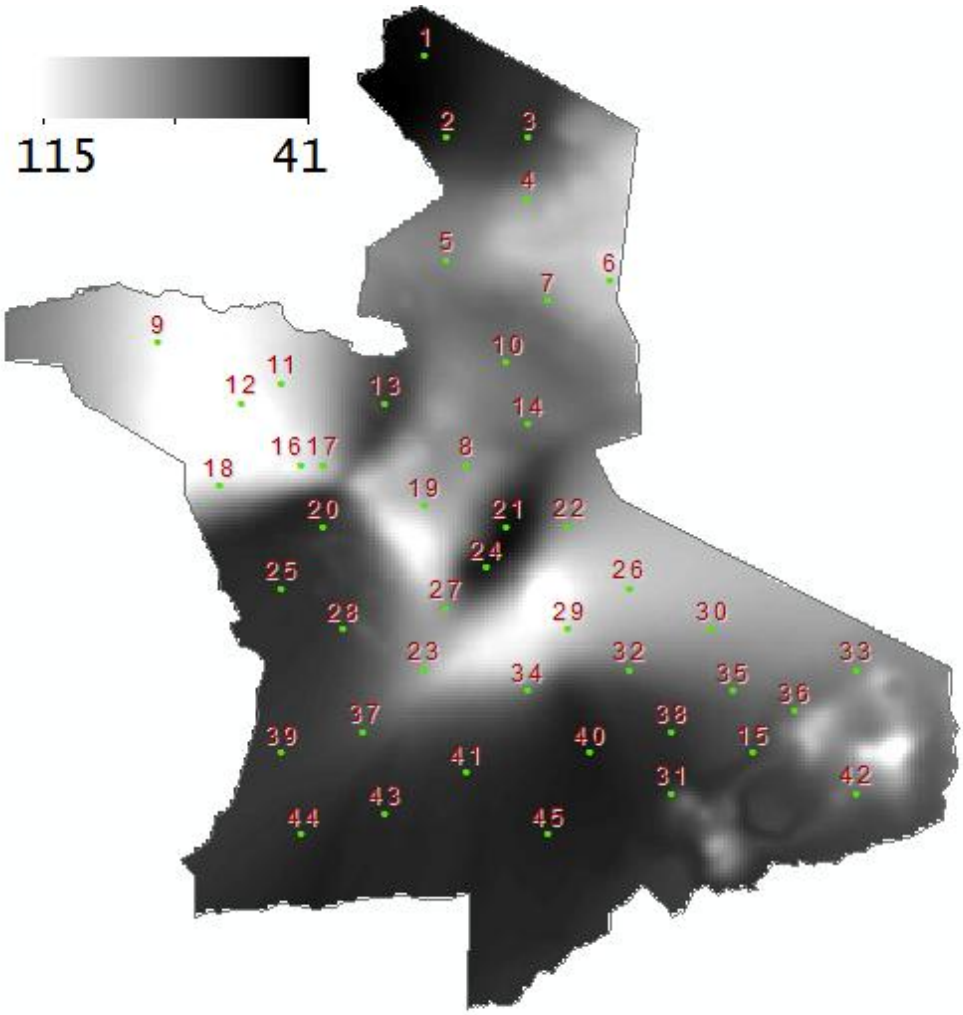


**a**

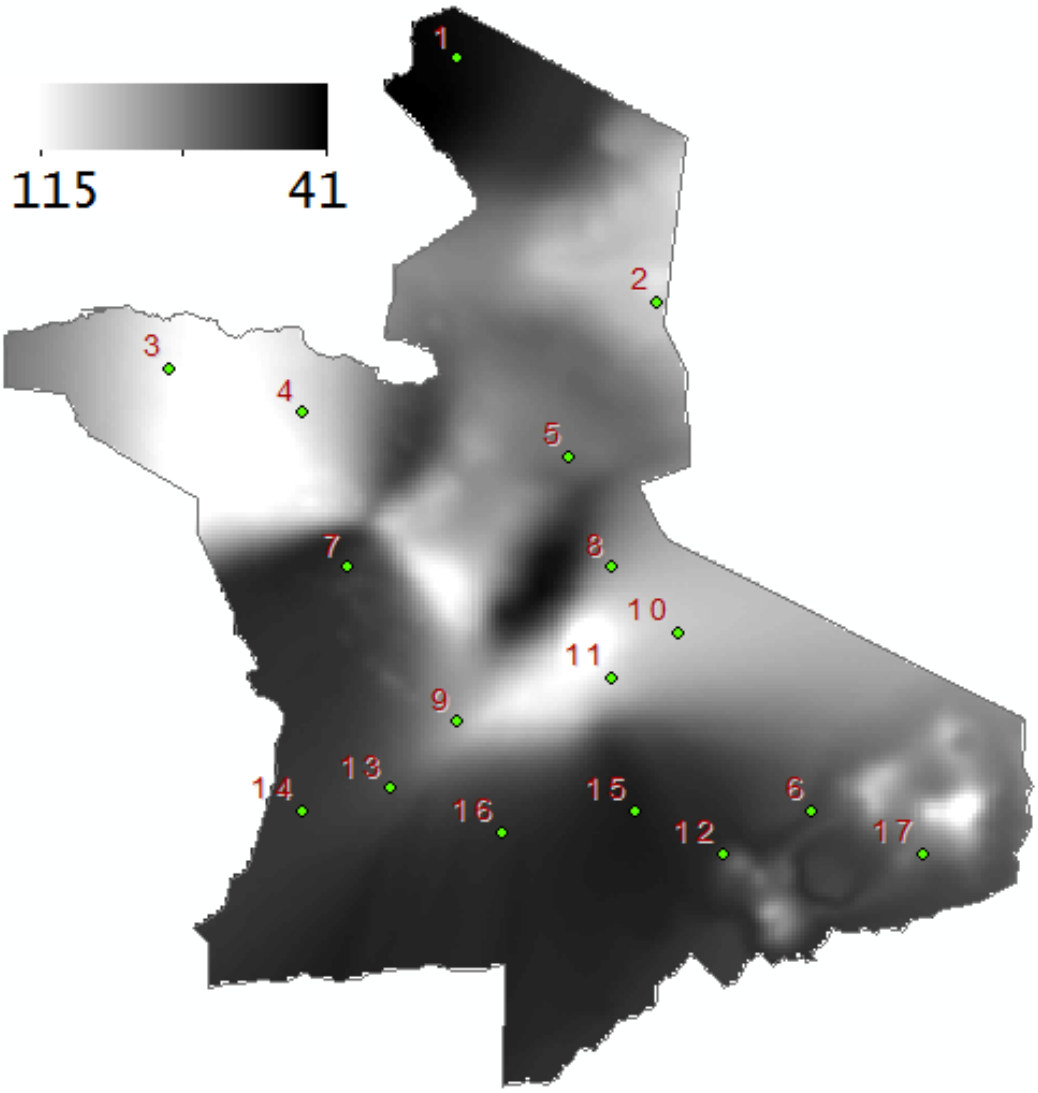


**b**

Fig. 14 Spectrum of 17 selected pixels; horizontal axis is the cycles indicated by the length of their period, vertical axis is the magnitude; the number above each figure is the number of the pixel; the value of PC1 and PC3 of the pixel is on the right side of the figure

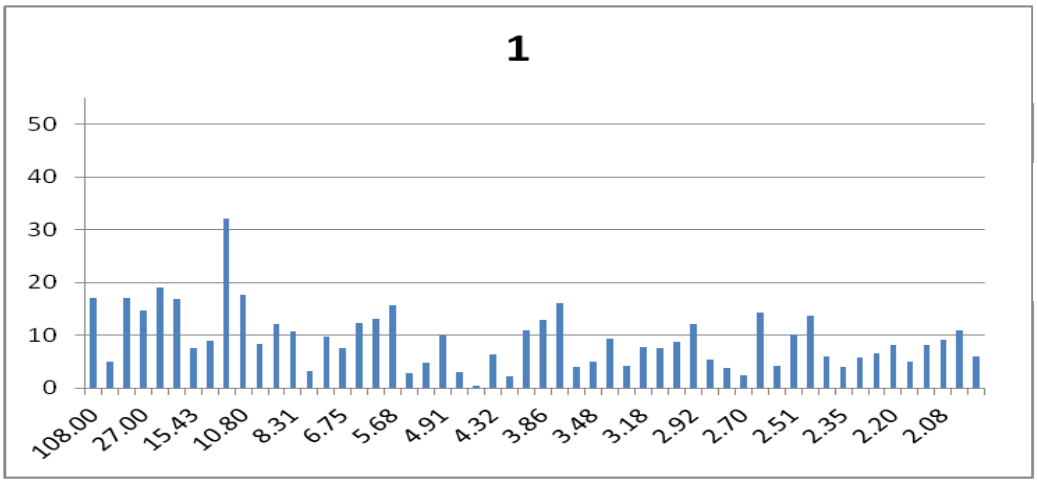


PC1

43.864

PC3

-42.352

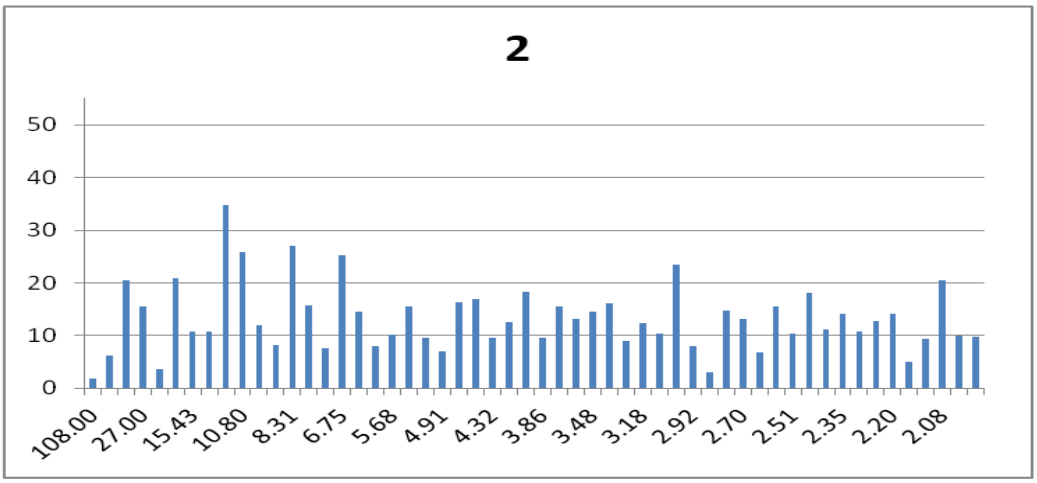


PC1

91.019

PC3

-16.640

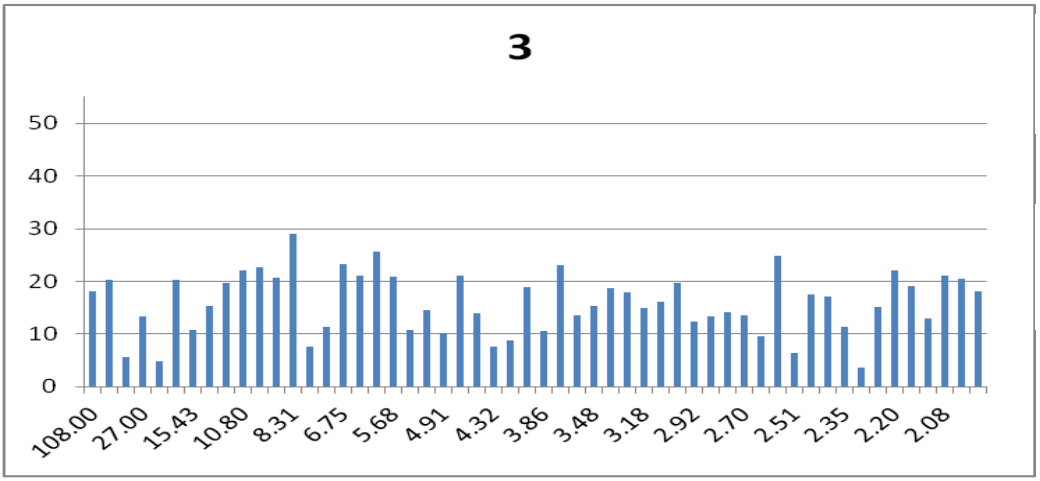


PC1

101.632

PC3

-17.229

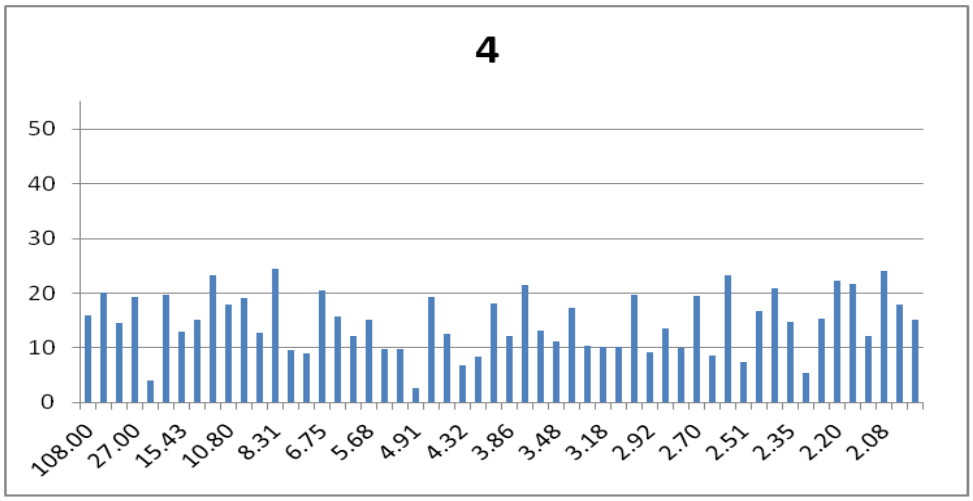


PC1

96.708

PC3

-19.556

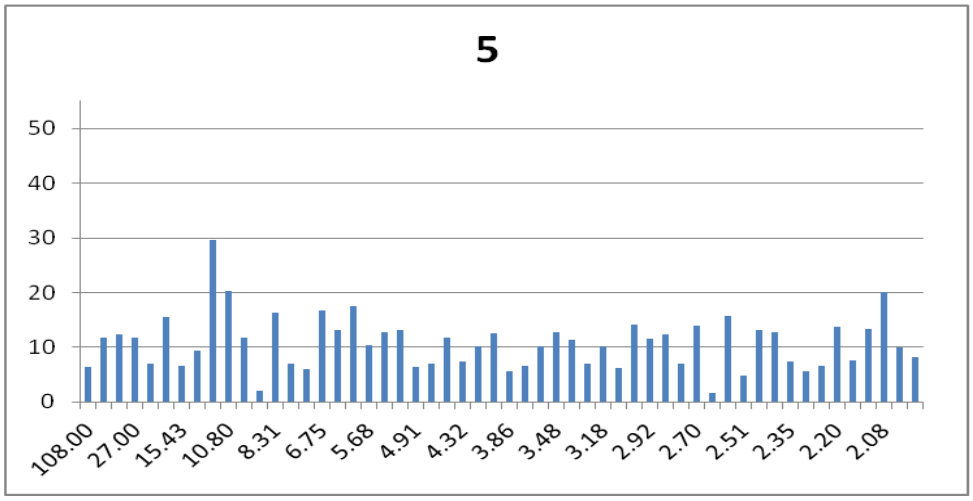


PC1

68.244

PC3

-12.291

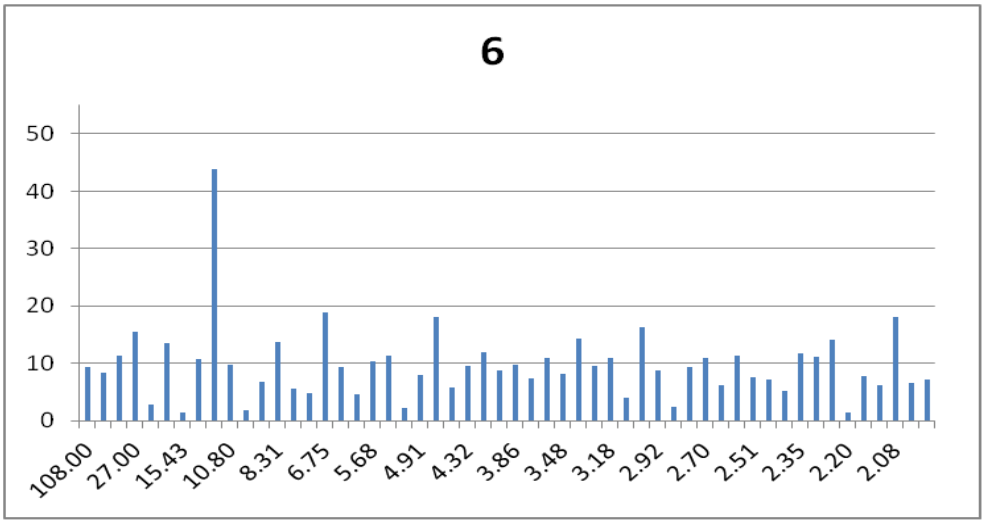


PC1

57.039

PC3

-14.976

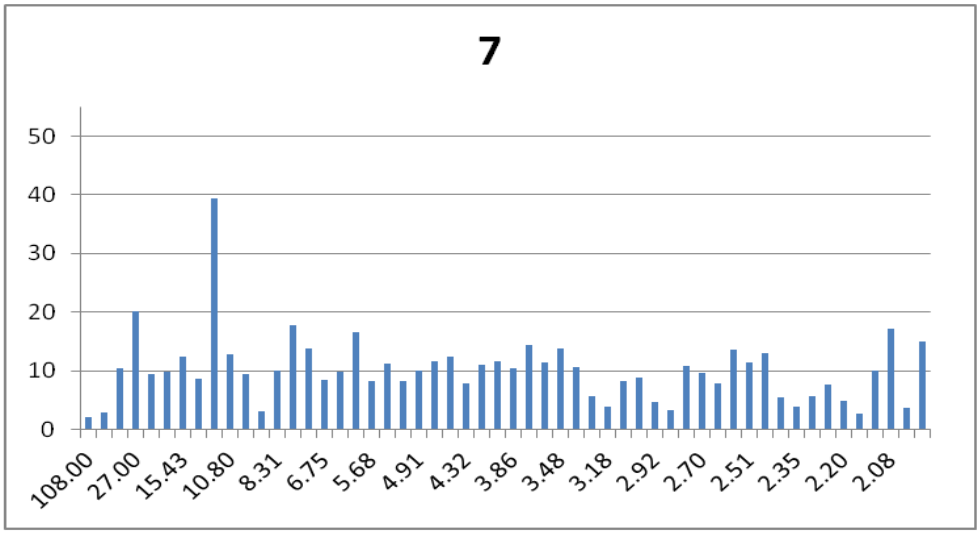


PC1

54.029

PC3

-15.648

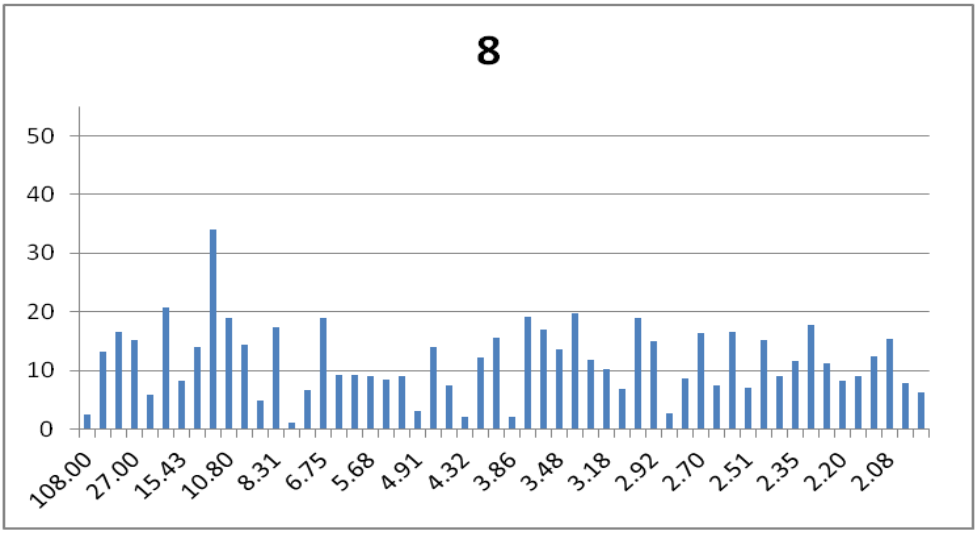


PC1

78.485

PC3

-15.142

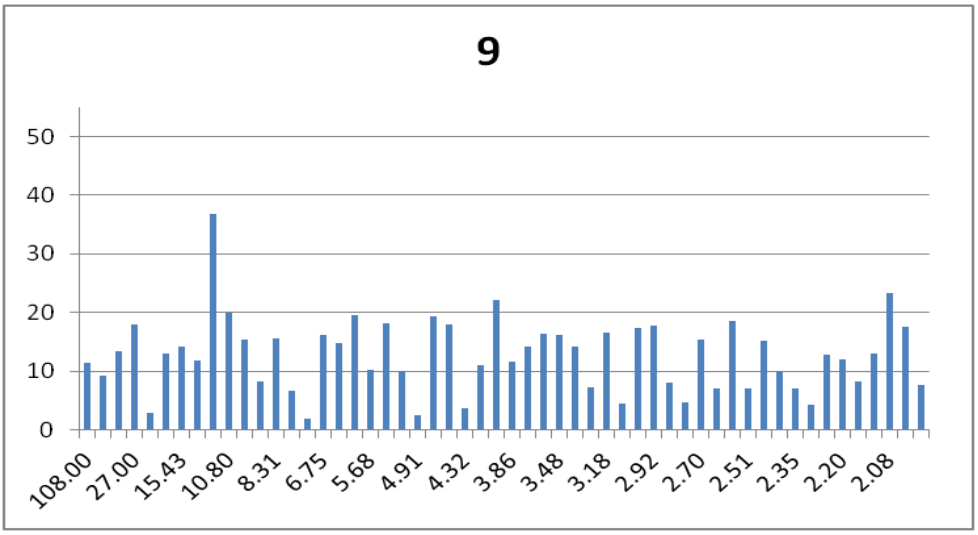


PC1

81.298

PC3

-14.436

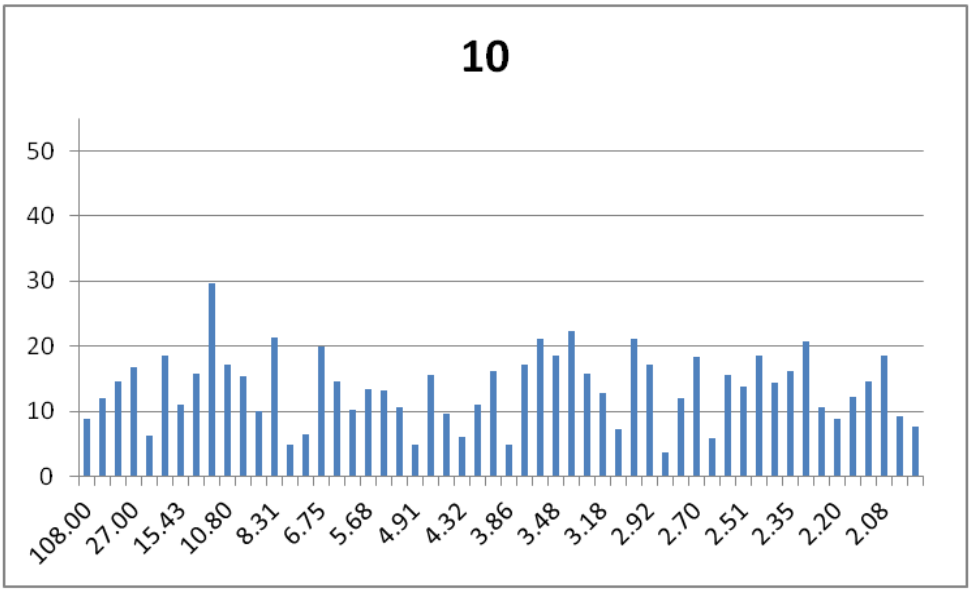


PC1

89.541

PC3

-13.918

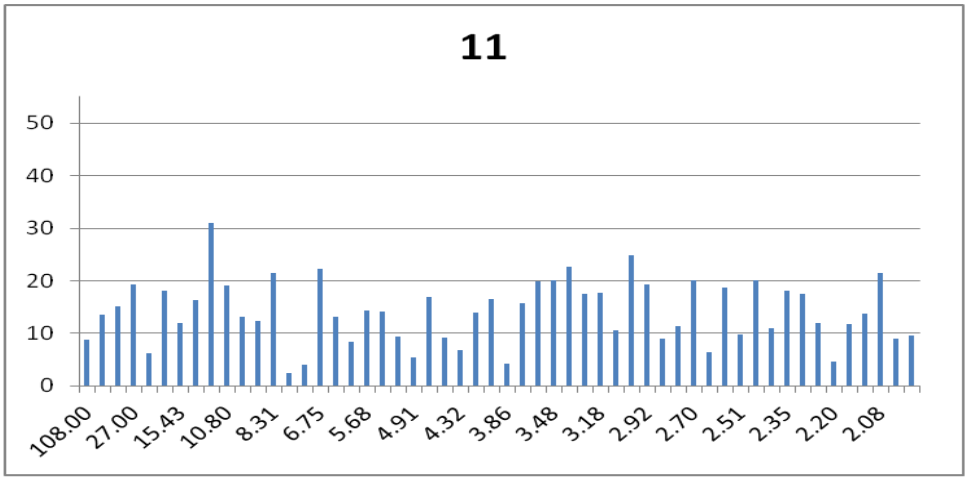


PC1

93.555

PC3

-13.511

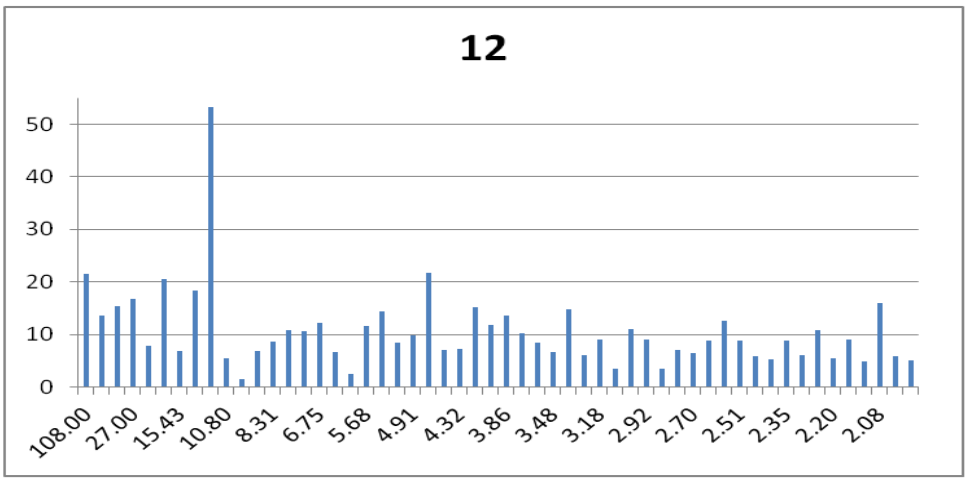


PC1

55.810

PC3

-32.676

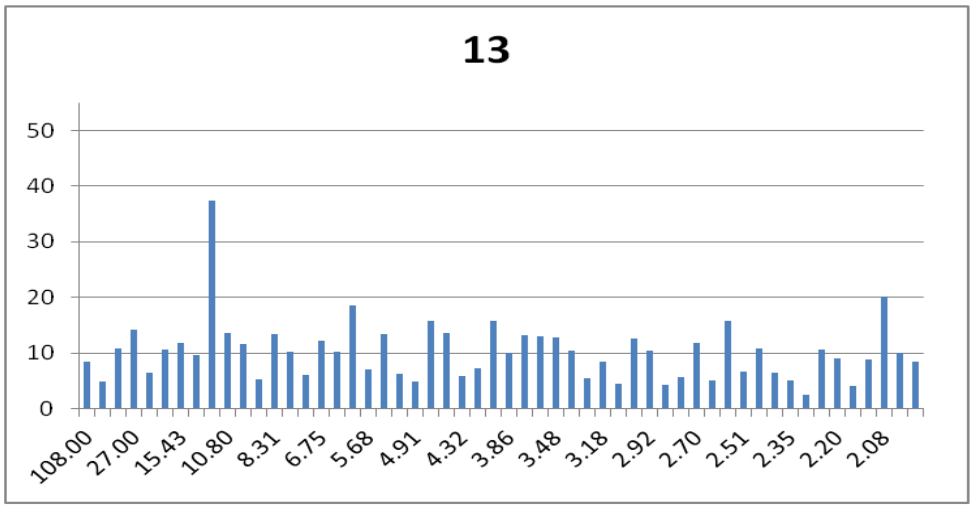


PC1

60.103

PC3

-13.137

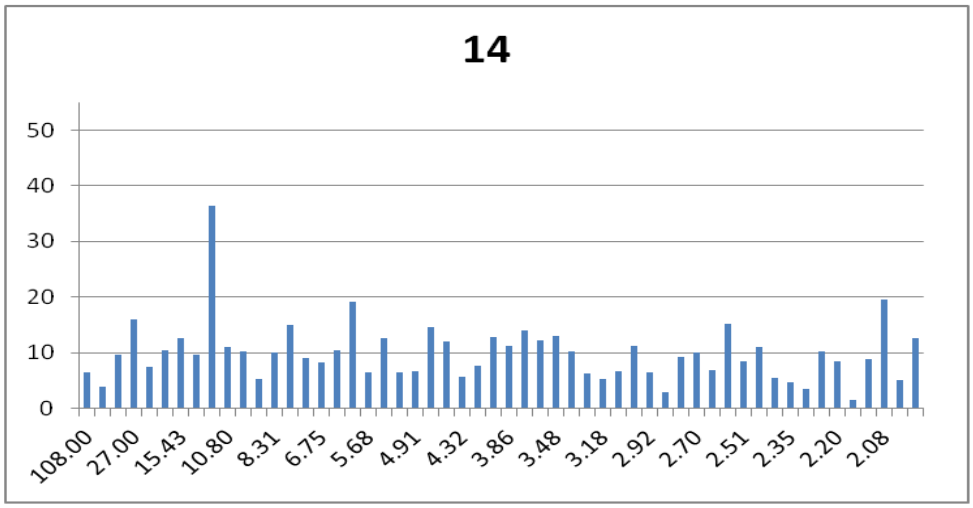


PC1

54.846

PC3

-12.353

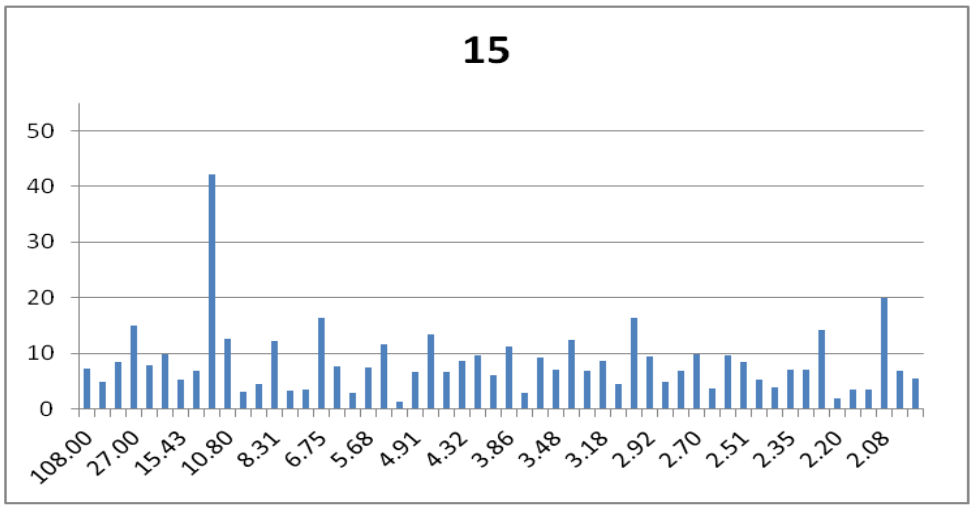


PC1

48.242

PC3

-14.515

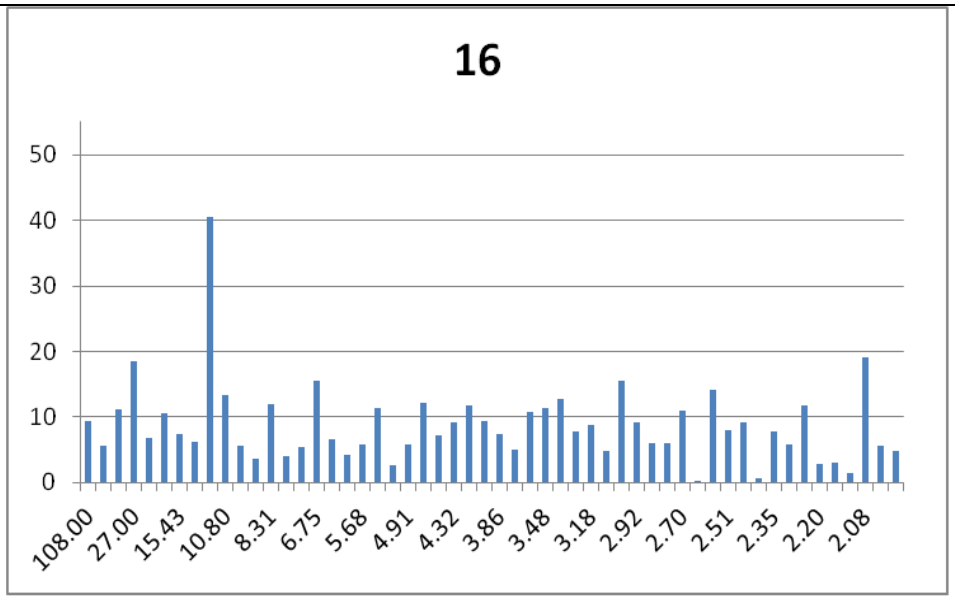


PC1

52.242

PC3

-13.879

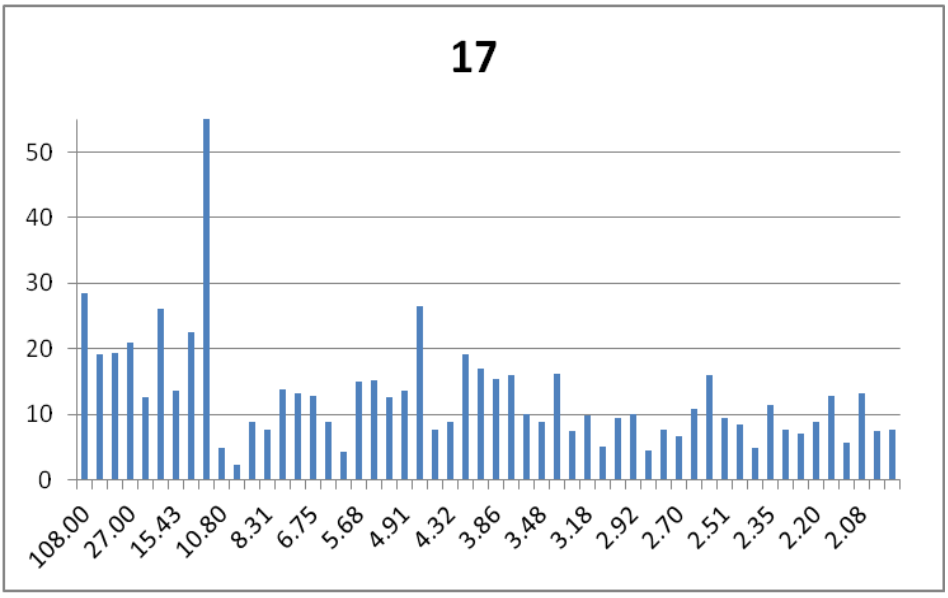


PC1

66.458

PC3

-43.059

Table 1 Percentage var. of PCA components

| PCA COMPONENT | % var. |
|---|---|
| PC 1 | 32.0836 |
| PC 2 | 21.9847 |
| PC 3 | 18.9642 |
| PC 4 | 6.0519 |
| PC 5 | 4.0280 |
| PC 6 | 3.0011 |
| PC 7 | 2.0170 |
| PC 8 | 1.1061 |
| PC 9 | 1.0405 |
| PC 10 | 1.0828 |
| PC 11 | 1.0094 |
| PC 12 | 0.8931 |
| PC 13 | 0.8728 |
| PC 14 | 0.7010 |
| PC 15 | 0.5611 |
| PC 16 | 0.5293 |
| PC 17 | 0.4317 |
| PC 18 | 0.3761 |
| PC 19 | 0.3100 |
| PC 20 | 0.2881 |

Fig. 15 Percentage variation explained by each PCA components

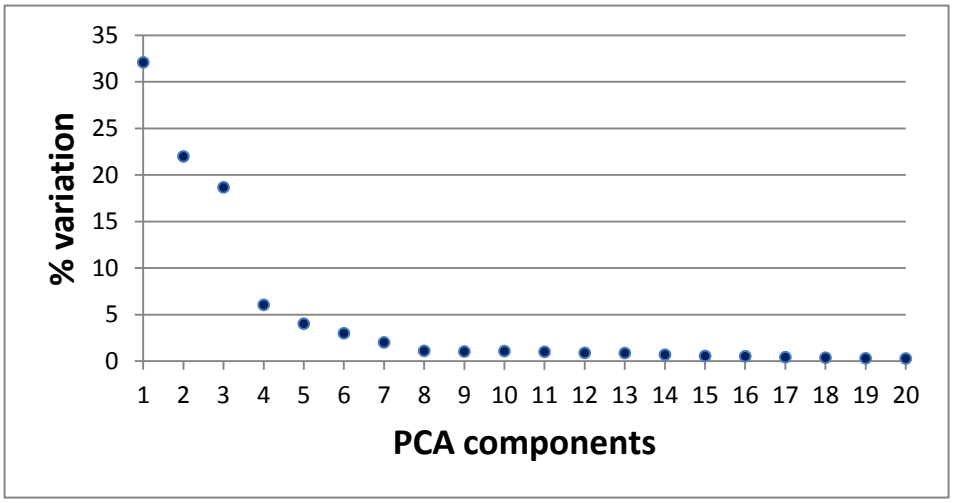

Fig. 16 The first three components of PCA analysis of the variation of precipitation

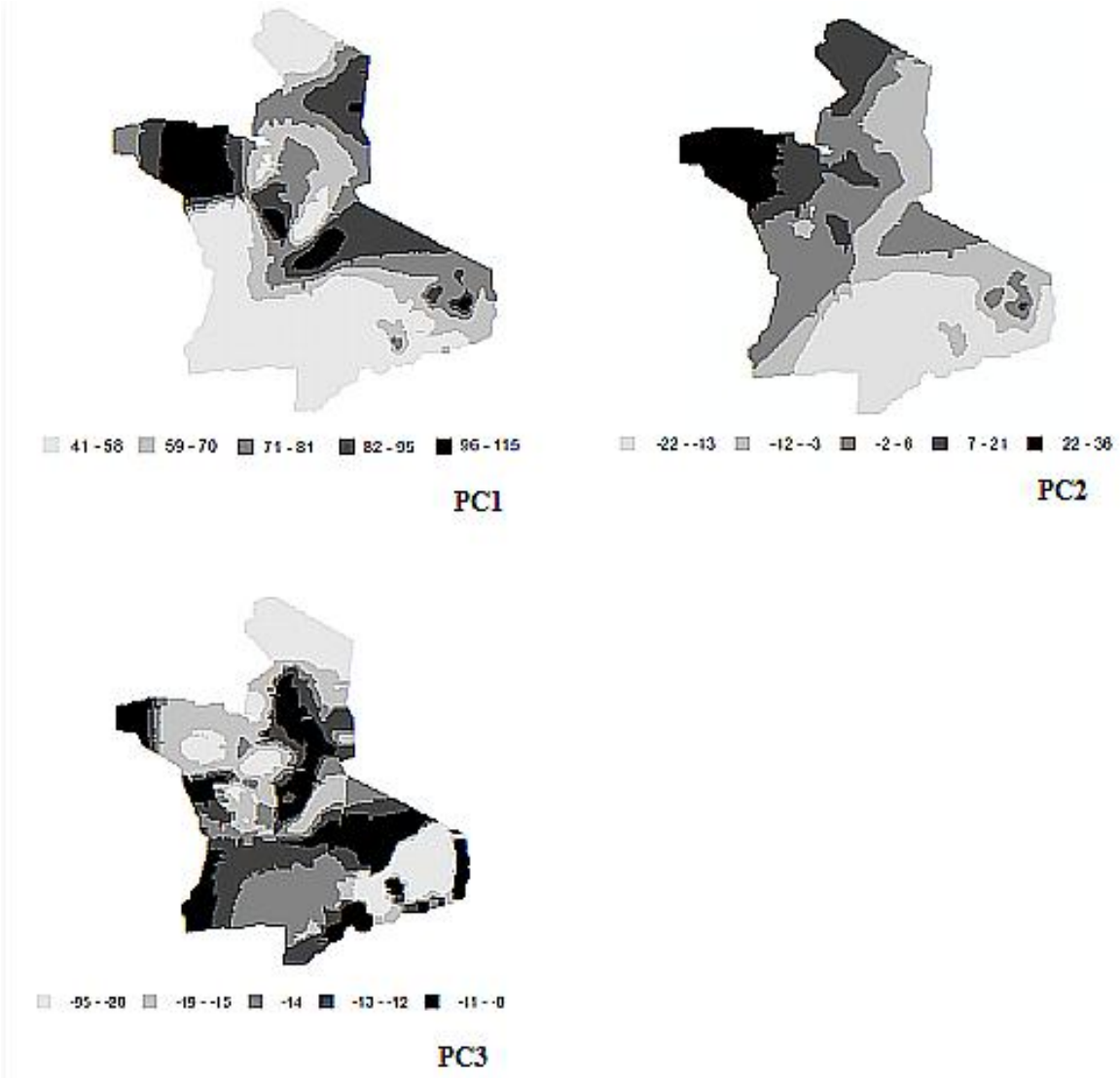

Fig. 17 Loadings of first three PCA components

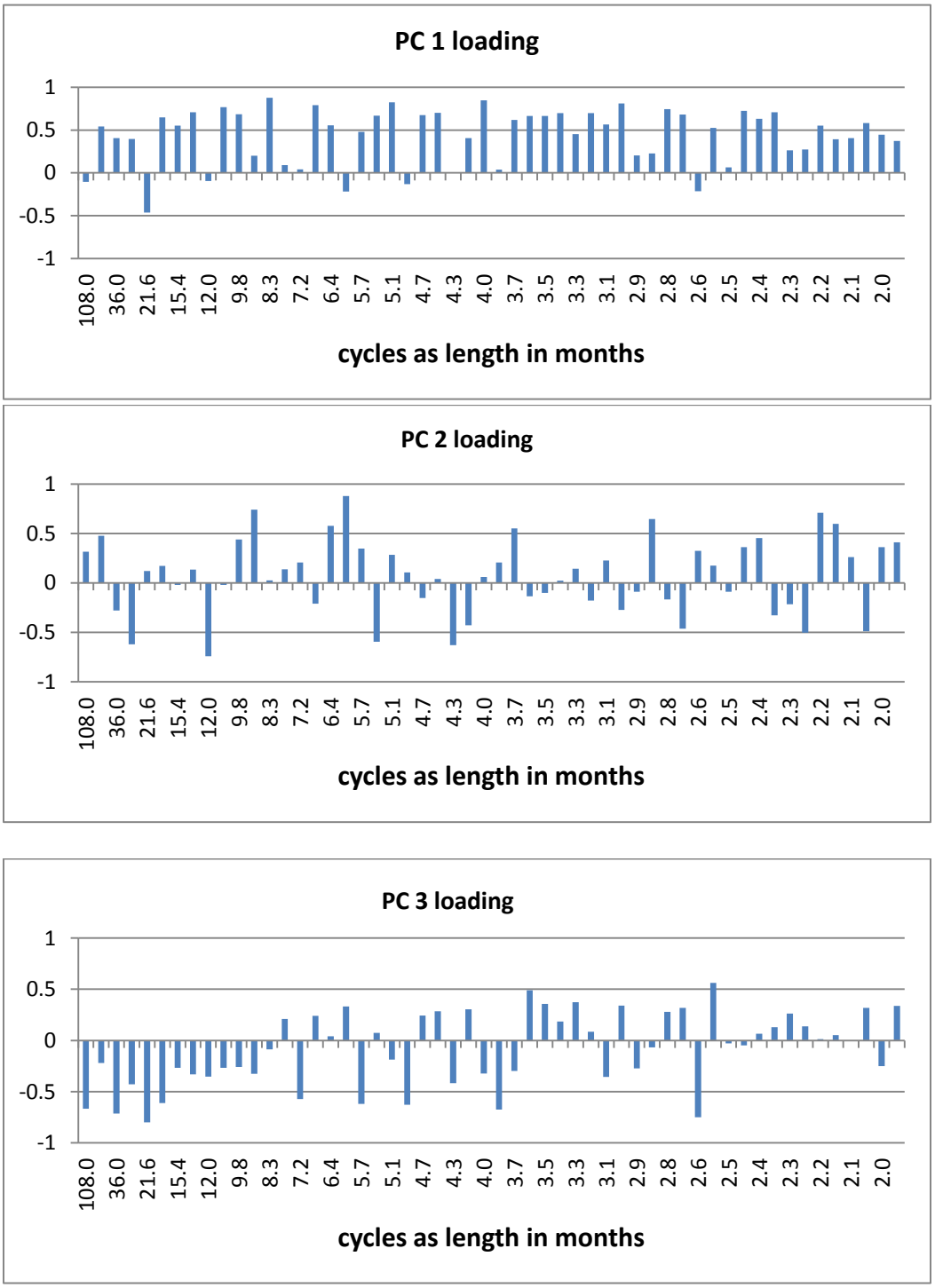

## *4.3 Global model of precipitation and mean EVI*

The map of the residuals of the OLS model (Figure 18a) shows that Northern SNP has high negative residuals. The residuals of the south-east part of SNP (NCAE and NCAE plain) show great variance. In the far south-east (NCAE region), the residuals are highly positive, but quickly become highly negative when moving towards the north-west. The rest area of SNP has intermediate/low residuals.

From the Q-Q normal plot (figure 18b), it appears that the residuals have a mean of approximately zero, but are not normally distributed. This is also confirmed by the corresponding p-value (0.0000) of the Jarque-Bera test's JB value, the statistical measurement of skewness and kurtosis (table 2). Moran's I is a measure of spatial autocorrelation with positive value indicates positive autocorrelation, negative value as negative autocorrelation and near zero as no correlation. The positive value of Moran's I here I indicates that the residuals are slightly positively autocorrelated. Thus the spatial distribution of residuals is both non-stationary and autocorrelated.

All independent variables have very high positive Moran's I; the Moran's I of mean EVI is 0.8320. This together with the largely reduced spatial autocorrelation of residuals indicate that the autocorrelation of mean EVI is mostly caused by the autocorrelation of independent variables. Based on corresponding p-values of a t test of the factors, it appears that both mean precipitation and the variation of precipitation make a significant contribution to model fitting. Mean precipitation has a positive impact on mean EVI. Both PC1 and PC3 have a negative correlation with mean EVI, but mean EVI is more sensitive to PC3. The p-value of the Joint F-Statistic further indicates that the overall model is significant.

Fig. 18 Diagnostic outcomes of the global model of precipitation-EVI relation

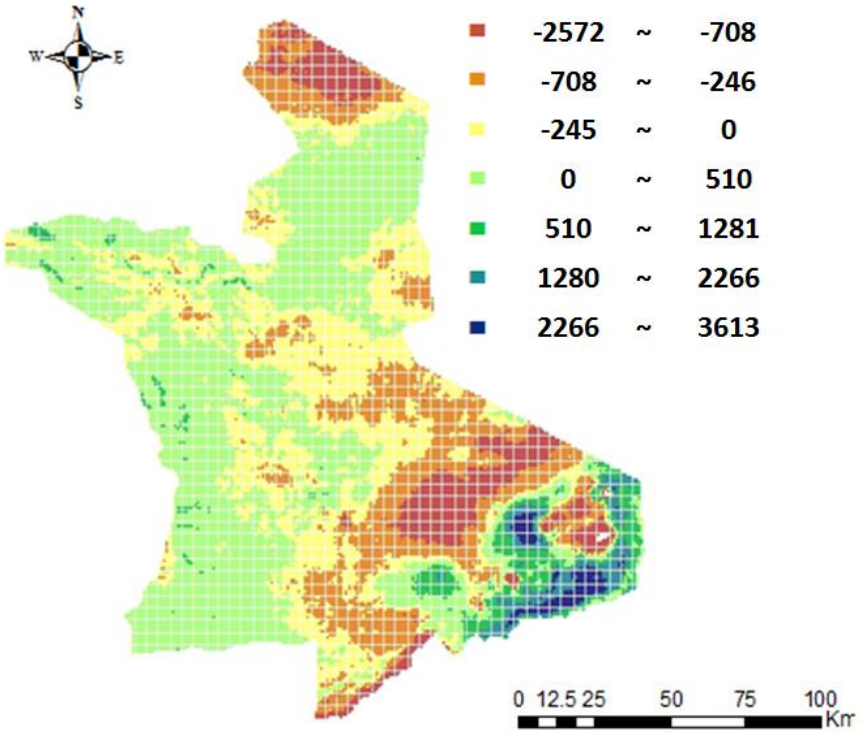


a. map of residual

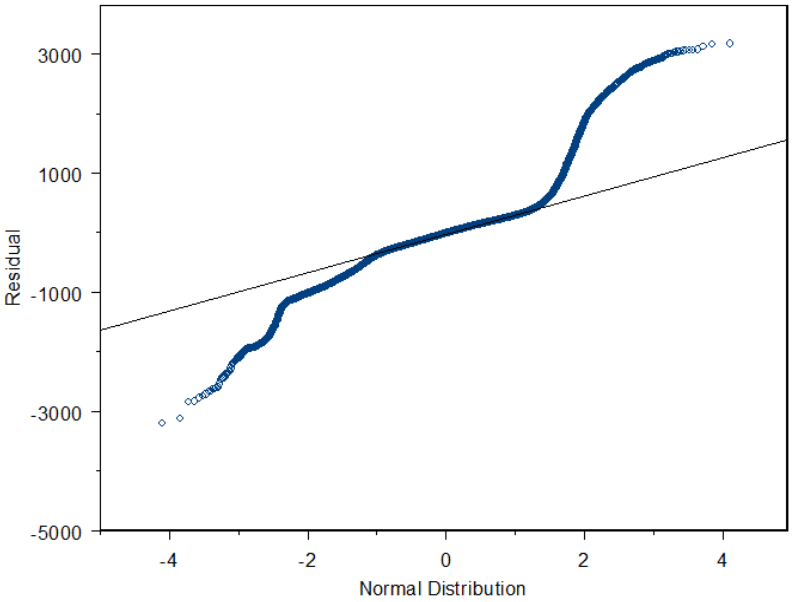


b. Q-Q plot of the residual

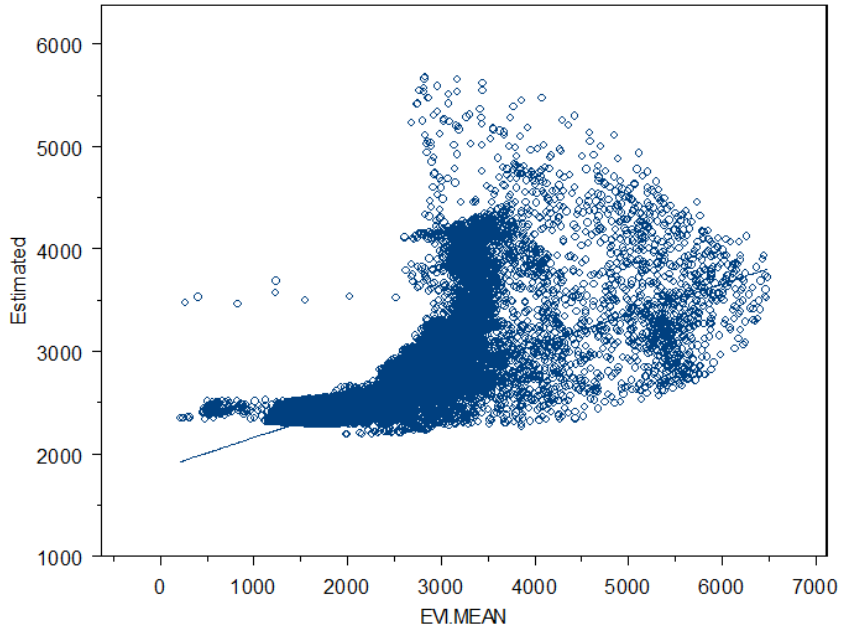


c. predicted vs. observed EVI

**Diagnostic statistics**

Joint F-Statistic: Prob (>F) = 0.0000 ***overall model is significant***

Koenker (BP) Statistic: Pr (>chi-squared) = 0.0000 ***unbiased standard errors***

Jarque-Bera Statistic: Pr (>chi-squared) = 0.0000 ***residuals are not normally distributed***

Residual Moran's I : 0.096 (z value: 214.93; p value: 0.0000) ***highly positively autocorrelated***

Table 2 Model Description

| **Factors** | **Coe. Value** | **Pr(>\|t\|)** | **Moran's I** |
|---|---|---|---|
| Intercept | 1296.78 | 0.0000 | |
| PPN_MEAN | 18.23 | 0.0000 | 0.9478 |
| PPN_PC1 | -3.85 | 0.0000 | 0.9453 |
| PPN_PC3 | -34.33 | 0.0000 | 0.8915 |

**$R^2$ = 0.392**

## *4.4 GWR outcomes of precipitation and mean EVI*

Three GWR models are created, namely GWR1, GWR2, and GWR3. Mean EVI is the dependent variable of all three GWR models. The independent variables used in each model are: mean PPN for GWR1, PC1&3 of PPN for GWR2, and mean PPN, and PC1&3 of PPN for GWR3. The outcomes of these GWR models (local $R^2$, coefficients, and t-value) describe the spatial non-stationary relation between mean EVI and the mean precipitation and the variation of precipitation. The variation of precipitation is described by PC1 and PC3 together. The loadings of these two PCA components denote the specific forms of variation, and the corresponding input layers, namely PC1 and PC3, represent the similarity of the variation of precipitation at each pixel to the pattern of PPN variation described by PC1 and PC3 values at that pixel.

Figure 17 shows the local $R^2$s and the residuals of three GWR models, which together tell how well mean EVI is explained by each of the mean and the variation of precipitation and by both together (high local $R^2$ and low residual means an explanatory factor well explains the variation of the dependent variable). The highest local $R^2$s of GWR1 occur at the north of SNP, and then decrease towards the west and east, with the lowest local $R^2$ occurring in south-east regions (figure 17a). Figure 17b shows that the highest local $R^2$s of GWR2 are in the north of SNP and the south-east regions, and decrease towards the north and west. Over all, the local $R^2$s of GWR2 are lower than those of GWR1 of the entire SNP. The local $R^2$s of GWRs are maximized at the west side of northern SNP and decrease towards the south-east. Through comparing figure 17a and figure 17b, we can see that the variation of precipitation is able to explain more variation of mean EVI than mean precipitation in south-eastern regions. Though the residuals of three GWR models vary in different ranges, they all have both large positive and large negative values in south-east regions, the NCAE and NCAE plains, and have low values in

the rest of SNP. For all three GWR models, the residuals show more spatial variation than the local $R^2$s (figure 19d,19e, 19f).

Figure 20 shows the coefficients and t-values of each independent variable (mean, PC1, and PC3 of precipitation) of GWR3. The coefficients of all three independent variables show clear spatial patterns (figure 20a,20b, and 20c). The coefficient of mean precipitation is maximized in the south-western region and decreases towards the north and east, and all have positive values. This indicates that vegetation productivity increases quickly with increasing mean precipitation in the south-western region and the increasing slows down towards the north and east. The coefficients of both PC1 and PC3 are negative; this indicates that the mean EVI decreases with the increasing of the similarity of the variation of precipitation to the variations of precipitation described by the loadings of PC1 and PC3. The coefficient of PC1 is maximized in the northern SNP, and shows a decreasing trend towards the south; this indicates that the mean EVI is most sensitive to the change in the variation of precipitation in the northern SNP, and the sensitivity decreases towards the south. The coefficient of PC3 is maximized in the north-western part of SNP and decreases toward south-east with lowest value occur at the NCAE and the NCAE plain regions. From the t-values, it appears that both mean precipitation and PC1 have significant impact on the mean EVI in south-eastern regions, the western region, and the north boundary of SNP, but are not significant in the center regions (figure 20d, 20e). Thus mean precipitation and the similarity of the variation of precipitation described by PC1 have significant impact on the mean EVI in the center regions. PC3 has significant impact on mean EVI in far south-eastern regions, but the impact quickly becomes insignificant when moving towards the north-west, and then becomes slightly significant at the center SNP. In the rest of SNP, PC3 does not have significant impact (figure 18f). This indicates that the changes in similarity of the variation of

precipitation to that described by the loading of PC3 have significant impact on the mean EVI only in far south-eastern regions.

Fig. 19 local $R^2$ and residuals of three GWR model; a. local $R^2$ (PPNmean); b. local $R^2$ (PPN_PC1&3); c. local $R^2$ (PPNmean, PC1&3); d. residual (PPNmean); e. residual (PPN_PC1&3); f. residual (PPNmean, PC1&3);

**fig. 19a**

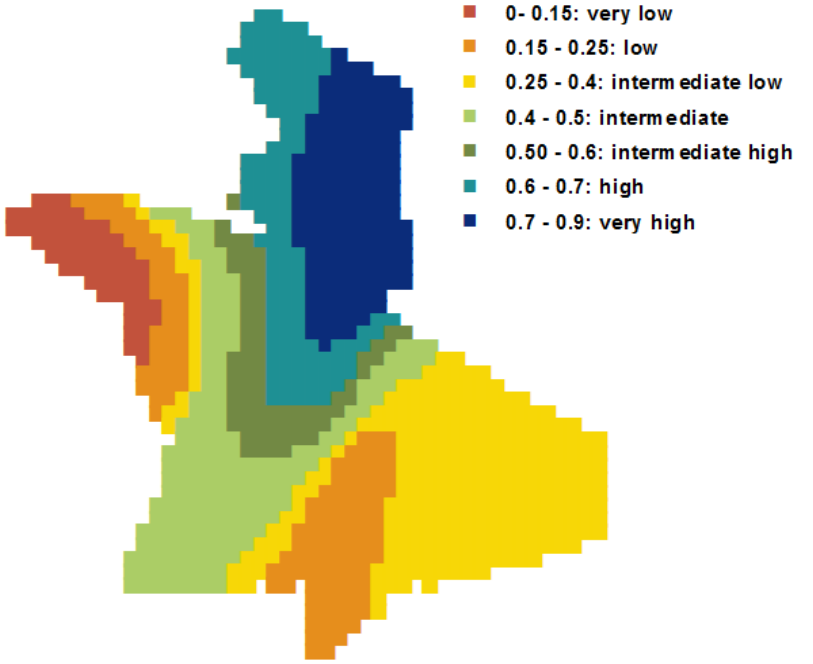


**fig. 19b**

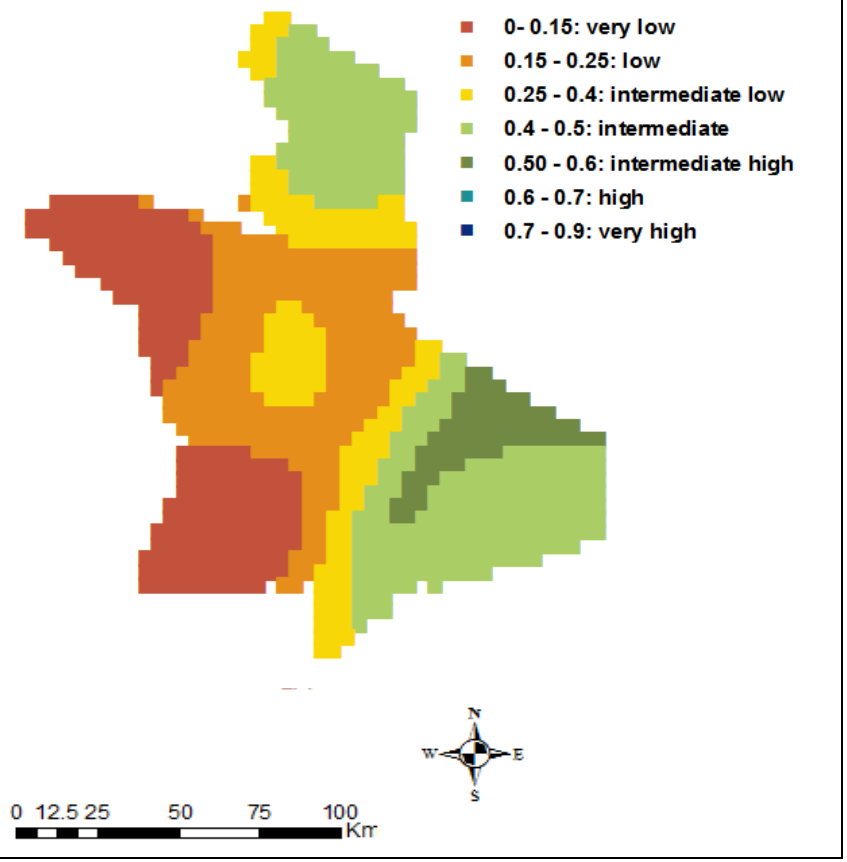

**fig. 19c**

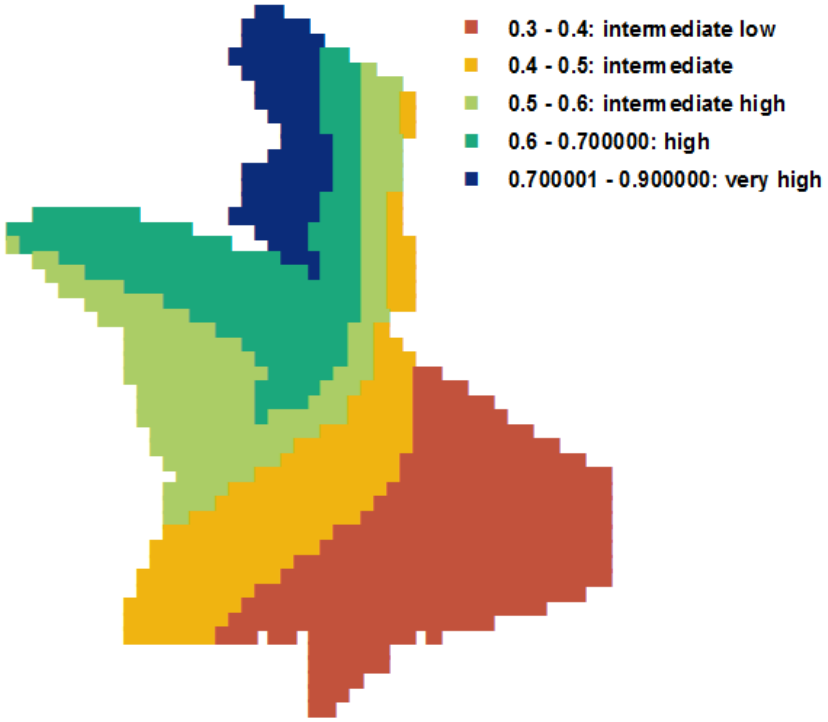


**fig. 19d**

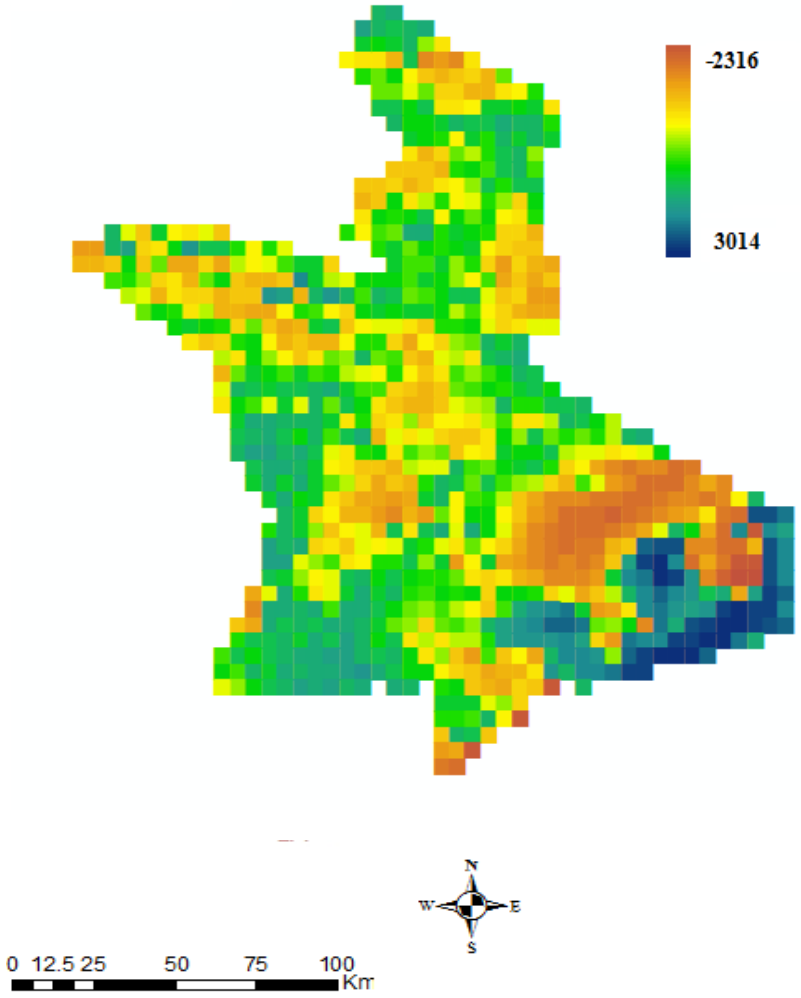

**fig. 19e**

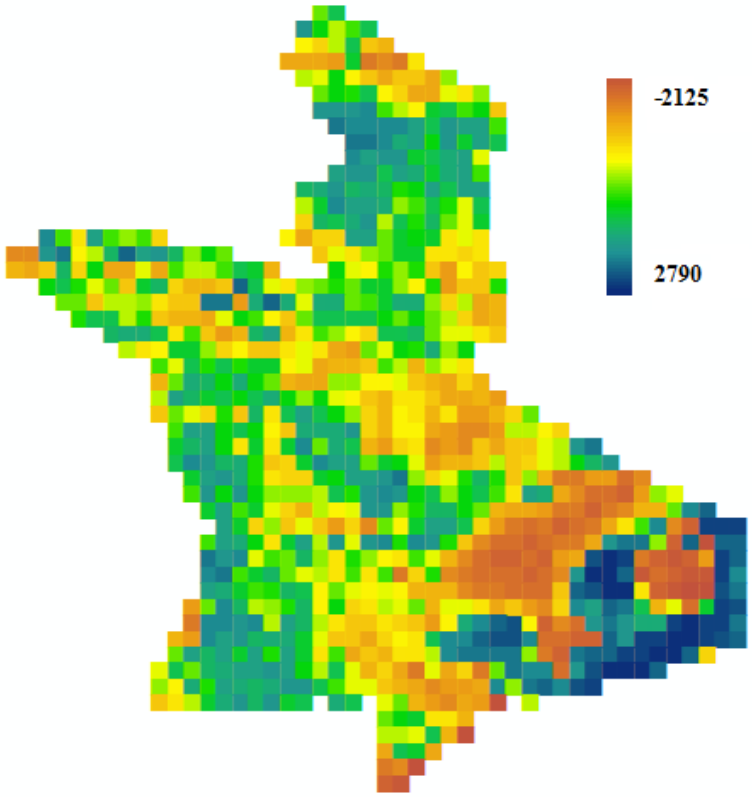


**fig. 19f**

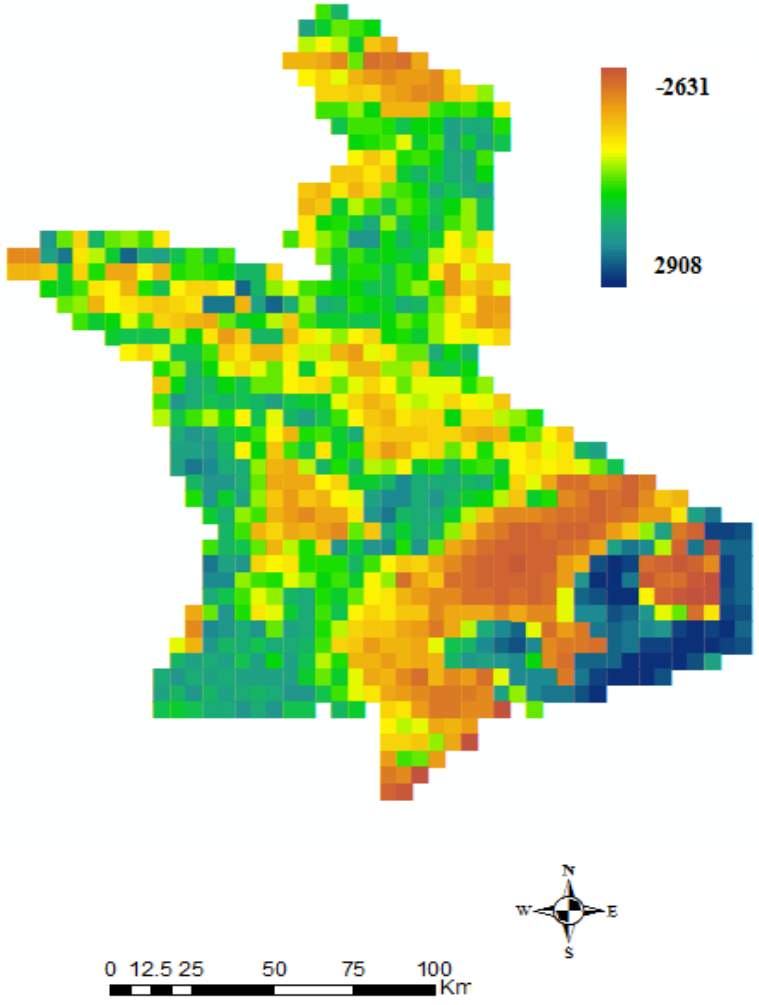

Fig. 20 Coefficient values and t-values of the independent variables of GWR3

**fig. 20a. Coe. PPN mean**

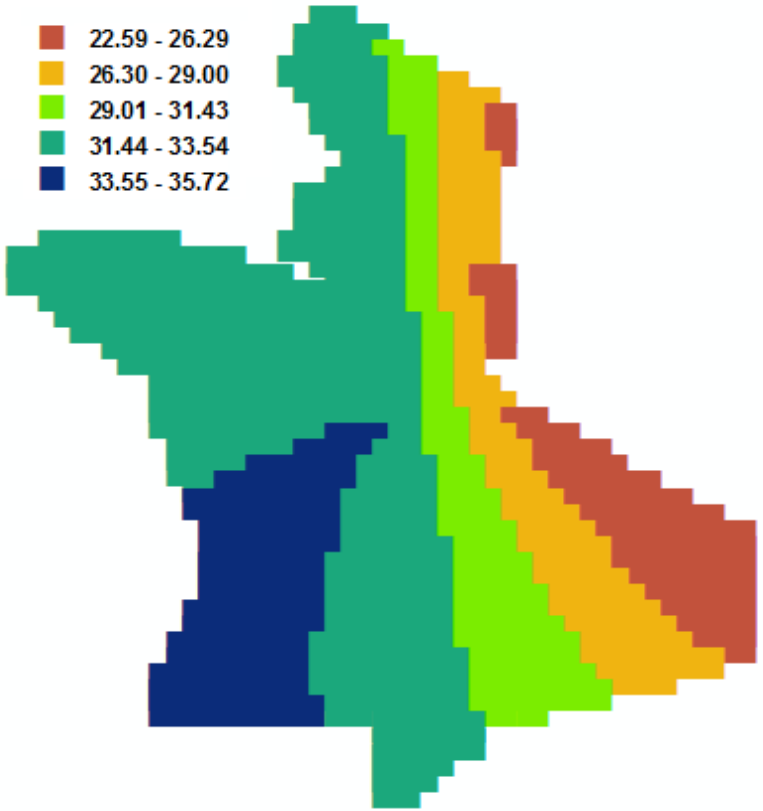


**fig. 20b. Coe. PPN PC1**

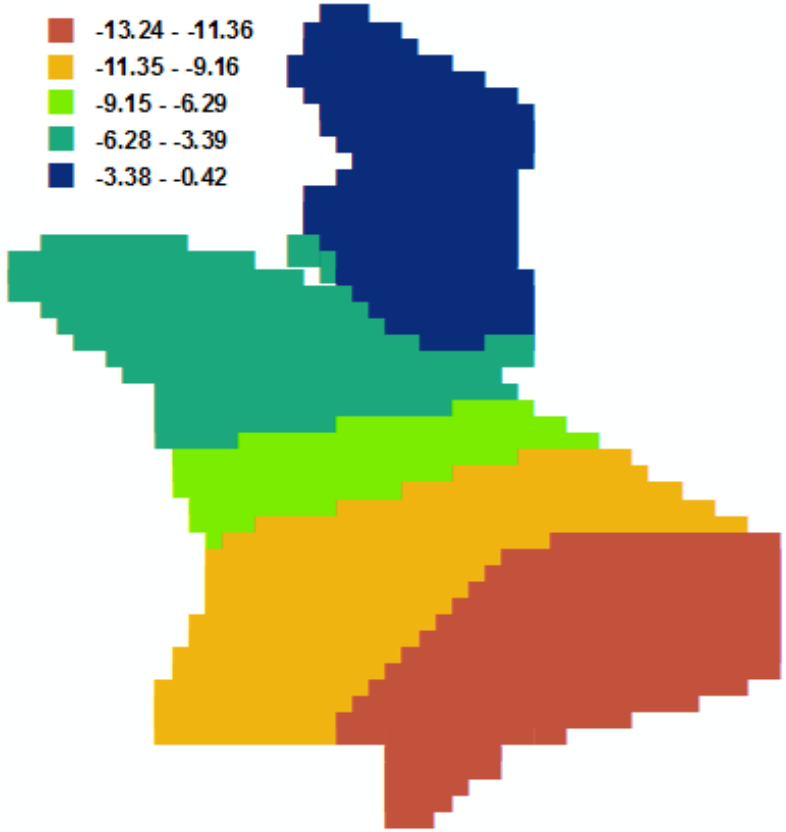

**fig. 20c Coe. PPN PC3**

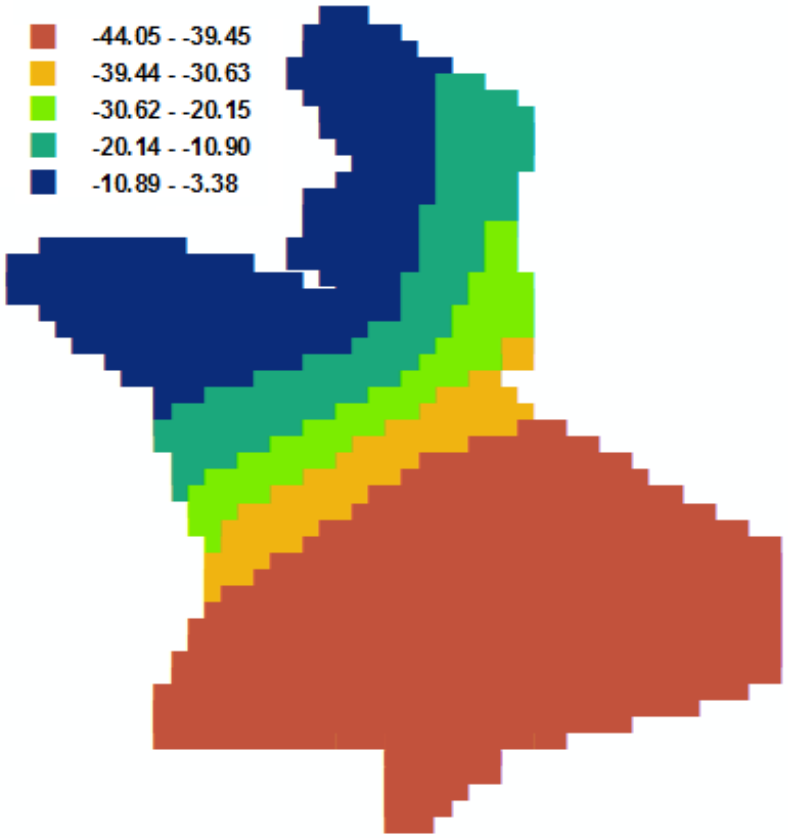


**fig. 20d t-value PPN mean**

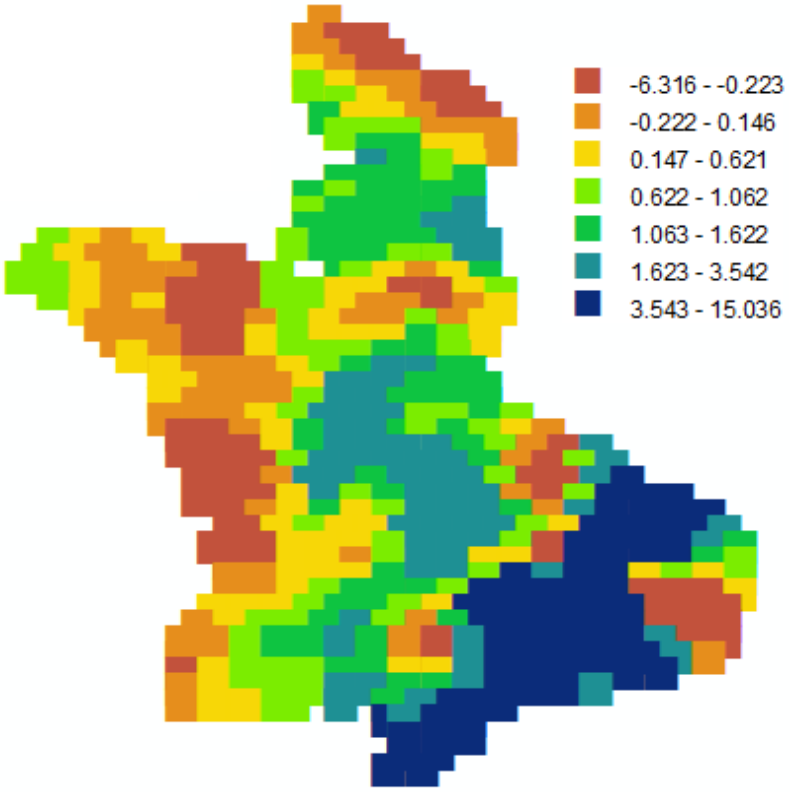

**fig. 20e t-value PPN PC1**

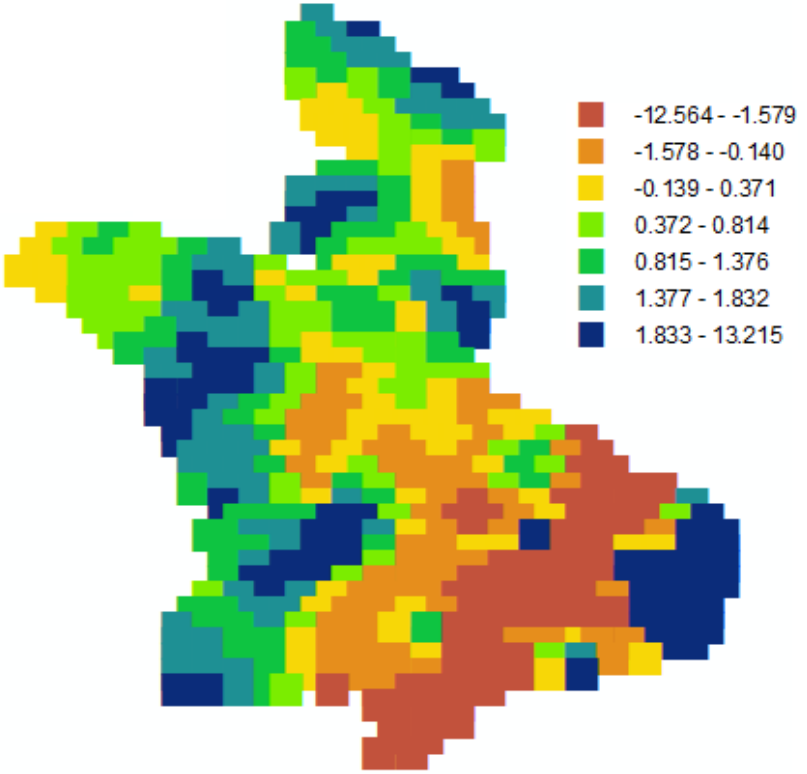


**fig. 20f t-value PPN PC3**

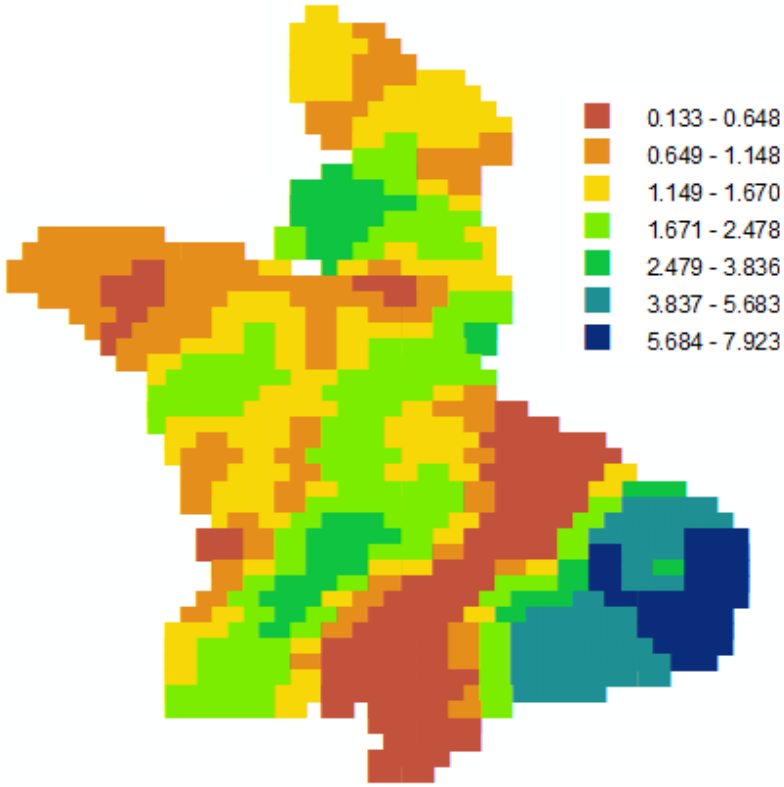

## *4.5 Impact of mean precipitation, soil WHC, N content, and vegetation on precipitation- mean EVI relations*

Table 3 is the outcome of three OLS models exploring the impact of mean precipitation, soil WHC, N content and vegetation type on the local $R^2$s of the corresponding GWR model. OLS1 looks how the ability of the mean precipitation to explain the variation of the mean EVI is affected by those geological variables. Based on the p-value of the t test of the independent variables of OLS1, it appears that both mean precipitation and Soil WHC have significant impact on the correlation between mean precipitation and mean EVI. Based on the coefficient values of mean precipitation and soil WHC, Local $R^2$ of GWR1 increases with mean precipitation, but decreases with soil WHC. This indicates that where mean precipitation is low, mean precipitation explains less variation of mean EVI; the portion of the variation of mean EVI explained by mean precipitation increases when mean precipitation increases. The p-value shows that land cover type does not have impact on the relation between mean precipitation and mean EVI.

OLS2 looks at how the ability of the variation of precipitation to explain the variation of mean EVI is affected by those geological variables. The p-values of OLS2 show that all three abiotic factors, mean precipitation, soil WHC and N content, have significant impact on the correlation between the variation of precipitation and the mean EVI. Results show that mean precipitation and soil WHC have negative impacts and soil N content has a positive impact on the relation. This means that the variation of precipitation explains less variation of mean EVI with increasing mean precipitation and/or soil WHC, but explains more variation with increasing soil N content. From the p - value of the t test, it appears that forest, woody savanna, and savanna

have significant impacts on the ability of the variation of precipitation to explain the variation of mean EVI. In other words, vegetation productivity in wetter areas appears more limited by soil N content than by precipitation. Vegetation type is treated as dummy variable. The coefficient of forest (0.1137) indicates that the local $R^2$ of GWR2 in forest is 0.1137 higher than the average. The coefficients of woody savanna (-0.1195) and savanna (-0.0952) indicate that the local $R^2$ of GWR2 in woody savanna is 0.1195 less than the average, and is 0.0952 less in savanna. The corresponding coefficients of these three vegetation type indicate that the variation of precipitation can explain more variation of mean EVI in the forest, but less variation of mean EVI in woody savanna.

OLS3 examines the impact of those geological variables on the ability of their means and variations together to explain the variation of mean EVI. The p-value of the t test shows that all mean precipitation, soil WHC and N content have significant impact; among the five vegetation types, the impact of forest, woody savanna, and savanna are significant. The coefficients indicate that precipitation is able to explain more variation of mean EVI when mean precipitation is high, but explains less variation when soil WHC is high. The coefficient of soil N is nearly zero. This is because the coefficient is non-standardized. This can alsoindicates though the impact of soil N content is significant, the variation of the goodness of fit is not very sensitive to the change of soil N content. The corresponding coefficients indicate that the mean and the variation of precipitation together explain less variation of mean EVI in the forest (-0.0157), but is able to explain more variation of mean EVI in both woody savanna (0.0178) and savanna (0.0175).

Table 3 OLS model outcomes

**OLS1 output**

| Factors | Coe. Value | Pr(>\|t\|) |
|---|---|---|
| PPTmean | 0.0042 | 0 |
| SOILWHC | -0.0034 | 0 |
| SOILN | 0 | 0.1732 |
| forest | 0.02607 | 0.5185 |
| shrub land | -0.0745 | 0.27 |
| Woody savanna | -0.0053 | 0.8759 |
| savannas | -0.0066 | 0.8303 |
| grassland | -0.0443 | 0.144 |

**$R^2$: 0.2769**

**OLS2 outputs**

| factors | Coe. Value | Pr(>\|t\|) |
|---|---|---|
| PPNmean | -0.0023 | 0 |
| SOILWHC | -0.0023 | 0 |
| SOILN | 0.0002 | 0 |
| forest | 0.1137 | 0 |
| shrub land | -0.0026 | 0.9655 |
| Woody Savanna | -0.1195 | 0.0001 |
| savanna | -0.0952 | 0.0006 |
| grassland | -0.0197 | 0.4675 |

**$R^2$: 0.3388**

**OLS3 outputs**

| Factors | Coe. Value | Pr(>\|t\|) |
|---|---|---|
| PPTmean | 0.0028 | 0 |
| SOILWHC | -0.0006 | 0 |
| SOILN | -0.00004 | 0 |
| forest | -0.0157 | 0.0134 |
| shrub land | -0.002 | 0.8561 |
| Woody savanna | 0.0178 | 0.0011 |
| savanna | 0.0175 | 0.0004 |
| grassland | 0.0012 | 0.8017 |

**$R^2$: 0.7263**

# 5. Discussion

The relationship between vegetation productivity and precipitation are spatially heterogeneous. For example, a few studies found that in Africa the best correlation between annual precipitation and vegetation productivity is reached at rain range 200 – 600 mm annual precipitation (Davenport and Nicholson, 1993; Nicholson et al., 1990; Camberlin et al, 2007). This indicates that the correlation between annual precipitation and vegetation productivity decreases when annual precipitation approaches 200mm and 600mm. Martiny and others (2005) discovered that the relation between precipitation and vegetation productivity can be described by a linear model but by different parameters for difference areas due to the variation of mean precipitation, soil properties and vegetation type. However, these studies are only conducted in small separately areas and the impacts of other geographical factors on the rainfall-vegetation productivity relation discovered are qualitative. In this project, the map of local $R^2$s of GWR1 provides continues and quantitative descriptions of the correlation between the mean precipitation and vegetation productivity. The local $R^2$s of GWR1 is much higher than the $R^2$s of the normal linear models used in previous studies. This is probably because GWR is able to count the variation of those geographical factors. The map of local $R^2$s further allows using regression model to discover the impact of mean precipitation, soil properties and vegetation type on the rainfall-vegetation productivity relation quantitatively which is described by the OLS1 model. The OLS1 model reveals a positive impact of mean precipitation on the local $R^2$ of GWR1. In a study, Propastinand Kappas (2008) uses GWR to explore the local correlation between precipitation and vegetation productivity in the middle part of Kazakhstan, a dry, cold and high continental region. They found that desert vegetation correlates much lower with the patterns of rainfall than steppe vegetation. In terms of precipitation, their study area is similar to

the south east of the Serengeti National Park. One reason is that there is a minimum requirement of water for plant to grow; Serengeti is a dry area, the precipitation there ranges from low to intermediate levels. In extremely dry regions, no plants can grow, thus there will be no correlation between precipitation and vegetation productivity there. Where precipitation exceeds the critical level, plants can grow and we will observe a correlation between precipitation and vegetation productivity. In areas with high mean precipitation, moisture is no longer a limiting factor to plant growth and there is less correlation again. This last situation is not common in Serengeti as it is a semi-arid ecosystem.

Though previous studies did not specifically look the impact of variation of precipitation alone on vegetation productivity, in one study Martiny et al. (2005) discovered that the previous year`s rainfall has an impact on current year NDVI, indicates that the inter annual fluctuation of precipitation can affect vegetation productivity. In this project, I apply PCA on the spectrums of precipitation to characterize its variation. According to the way the principle component is computed, there is no general method to figure out which kind of variation of real observation is captured by each component. However, by looking the spectrums of selected pixels together with the loading it appears that PC1 of the variation of precipitation may capture the part of the spatial variation of different cycles that are positively correlated which may be the combination of the certain characteristics: the variation of the relative dominance of annual cycle, the variation of overall magnitudes of all cycles, and the variation of the difference of magnitude of long cycles and short cycles. In this project, the PC1 tends to catches the variation of the magnitude of annual cycle. Thus, the negative value of the coefficient of PC1 of the global model on the rainfall-EVI relationship indicates that increasing the fluctuation, particularly the inter-annual fluctuation of precipitation may result in lower vegetation productivity. Future research can be

conducted to discover how above characteristics of the variation of precipitation may affect vegetation productivity in Serengeti ecosystem. PC2 is detected to be highly correlated with mean precipitation. There is one reason for this correlation. The loading of PC2 shows that PC2 captures the negative correlation between annual cycle and semi-annual cycles, the dominance of annual cycle or semi-annual over another. PC2 is negatively correlated with the magnitude of annual cycle and positively with semi-annual cycles. Thus the large PC2 value means the place is dominated by semi-annual cycles while small PC2 value means the place is dominated by annual cycles. Previous studies on the precipitation in SNP (Janowiak, 1988; Ropelewski and Halpert, 1987; 1989; 1996) found that the north region of SNP receives high precipitation and is also dominated by semi-annual cycle. Precipitation becomes lower and annual cycle dominates when moving towards south. Thus the relative strength of semi-annual cycle to annual cycles of the SNP is associated with mean precipitation.

In a study, Camberlin et al. (2007) found that when the available water capacity of soil exceeds 150mm, the response of vegetation productivity to precipitation variability becomes insignificant as soil moisture retention weakens the impact of precipitation variability. In this project, soil water holding capacity is found to have a negative impact on the relation between vegetation productivity and both the mean and the variation of precipitation. This is because, though the source of water comes from precipitation, plants actually obtain water from soil; thus soil acts as a temporary storage of water. Soil with high water holding capacity has a large storage capacity which makes vegetation productivity less sensitive directly to precipitation.

Although statistically grassland does not have an impact on the relation between precipitation and vegetation productivity, in south-eastern regions the combination of precipitation, soil and grassland can cause the mean EVI to be less correlated with mean

precipitation than with the variation of precipitation. Soil is thin and alkaline in south-eastern regions as it is affected by the underline geography, volcanic rock. This prevents the penetration of the roots of trees thus leading to the dominance of grassland in that region. This has two effects. First, thin soil has very low capacity to store water. In this case, the way precipitation occurs over time determines how much water can be used by plants. For example, suppose that two places receive the same amount of precipitation, but at one place precipitation occurs more aggregated in time, large rainfalls tend to occur together, and the other place has more episodic precipitation. Runoff is more likely to occur at the first place and consequently there is lower vegetation productivity at the first place. Second, trees have deeper root systems than grasses; thus trees can reach water stored at depth while grass can only use water stored within the surface layer of soil. The water content of the surface layer of soil fluctuates more with precipitation while the moisture of the deep soil is less affected by the variation of precipitation thus trees are capable to use the deep soil moisture that can be released over time (Propastin and Kappas, 2008). These two factors together determine that the vegetation productivity at that region is very sensitive to the variation of precipitation.

The effect of topography on EVI at SNP has not been extensively explored. Nippert and others (2011) conducted a study on a 3487 ha grassland and found that topography, characterized by the 1m resolution DEM, impacts vegetation productivity; they developed a model incorporating topography in a GWR model. However, their model is in a very small area, and the validity of the model in a large area has not been tested. Further exploration will be needed to understand the impact of topography on EVI at SNP.

GWR reveals the non stationary relation between precipitation and vegetation productivity at SNP. Previous studies identified that GWR model provide better statistic description of the

rainfall-vegetation productivity relation (Brunsdon et al., 1996; Wang et al., 2005; Zhao et al., 2010). However, these studies overlook the significance of stationary process. The outcome of the global model of this project indicates the stationary relation is also significant. In fact, the response of vegetation productivity to precipitation is the combination of both stationary and non-stationary processes. The source of the stationary relation comes from the mechanism that all the plants require water to grow, and the way that water is transported through the soil and absorbed by plants is governed by the same fundamental laws. The non-stationary force comes from the heterogeneity of the physical environment and the differences in the physiological structure of plants (e.g. root depth). Since the strength of GWR is to detect the non-stationary relation, the outcome of GWR may overlook or underestimate the stationary relation. Since OLS and GWR have their own advantages and are used to discover mechanisms (OLS is used to discover stationary relations, GWR is for non-stationary relations). This study shows that the relation between precipitation and EVI from OLS model is significant. Thus it will be more appropriate to compare the outcome of both OLS and GWR to understand to which extent each stationary and non-stationary process is valid, rather than identifying which model is better. For example, we can run the GWR model on the residuals of the global model, or vise versa, so that we can know which part of the variation can be explained by each of the stationary and non-stationary processes.

Finally, it needs to be noticed that I do not intend to look the impact of specific climatic events on the vegetation productivity but the impact of the variation of precipitation as described by the whole profile of the variation which is the result of the combination of different climatic events. Therefore, the findings of my project won't be able to relate to a specific climatic events like El Nino.

# 6. Conclusion

The relation between vegetation productivity and each of the mean and the variation of precipitation is non-stationary at SNP. Such non-stationary relation can be explained partly by the difference in average precipitation, soil properties and vegetation type. In this study, I demonstrate that we can quantitatively describe and explain the cause of such non-stationary relation by spatial statistics using MODIS EVI. The outcome of this study can provide useful information for agricultural management in that region.

The significance of the global model of the precipitation - vegetation productivity relation indicates that the stationary process is also important: the vegetation productivity in SNP is actually determined by the combination of the stationary and the non-stationary processes. Further studies are needed to understand how the combination of the stationary and the non-stationary processes affect the relation between precipitation and vegetation productivity.

In addition, this study shows that the variation of precipitation along described by selected PCA components can affect mean vegetation productivity. The shortcoming of PCA is that the PCA components do not have physical meanings. Thus further study is needed to link the PCA components to meaningful variation of precipitation. Also, the impact of topography needs to be explored.

# 7. References


Allen, T., Curtis, S., & Gamble, D., 2010, The midsummer dry spell's impact on vegetation in Jamaica. *Journal of Applied Meteorology and Climatology* 49(7): 1,590–1,595

Black E, Slingo J, & Sperber KR, 2003, An observational study of the relationship between excessively strong short rains in coastal East Africa and Indian Ocean SST. Mon Weather Rev 131:74–94

Brunsdon, C., Fotheringham, A. S. & Charlton, M. E. ,1996, Geographically Weighted Regression: A Method for Exploring Spatial Nonstationarity. Geographical Analysis, 28: 281–298.

Camberlin, P., Martiny, N., Philippon, N., & Richard, Y., 2007, Determinants of the interannual relationships between remote sensed photosynthetic activity and rainfall in tropical Africa, remote Sensing of Environment, 106 199–216

Chamaillé-Jammes, S. and Fritz, H., 2009, Precipitation-NDVI relationships in eastern and southern African savannas vary along a precipitation gradient, International Journal of Remote Sensing, 30: 13, 3409 — 3422

Cho, S.-H., Lambert, D. M., & Chen, Z. 2010. Geographically weighted regression bandwidth selection and spatial autocorrelation: an empirical example using Chinese agriculture data. *Applied Economics Letters* 17(8), 767-772.

Clark, CO, Peter J. Webster, and Julia E. Cole, 2003, Interdecadal Variability of the Relationship between the Indian Ocean Zonal Mode and East African Coastal Rainfall Anomalies, Journal of Climate Vol. 16, Feb. 2003

Coughenour, M. B. 1992, Spatial modeling and landscape characterization of an African pastoral ecosystem: a prototype model and its potential use for monitoring drought. pp. 787-810 in: D.H. McKenzie , D.E. Hyatt and V.J. McDonald (eds.). Ecological Indicators, Vol. I. Elsevier Applied Science, London and New York.

Cryer, Jonathan D. & Kung-sik Chan, 2008, Chapter 13: Introduction to Spectral analysis, in book: Time series analysis, Springer New York, 2008

Davenport, M. L. & Nicholson, S. E. 1993, On the relation between rainfall and the Normalized Difference Vegetation Index for diverse vegetation types in East Africa, International Journal of Remote Sensing, 14: 12, 2369 — 2389

FAO, 1995, The Digitized Soil Map of the World DSMW – version 3.5 CD

Farber, S., & Páez, A. 2007, A systematic investigation of cross-validation in GWR model estimation: empirical analysis and Monte Carlo simulations. *Journal of Geographical Systems* 9, 371-396.

Fotheringham, A.S., Brunsdon, C., & Charlton, M.E., 2002, *Geographically Weighted Regression: The Analysis of Spatially Varying Relationships*, Chichester: Wiley

Free World Maps, 2012, http://www.freeworldmaps.net/africa/index.html, last accessed May 18th. 2012

Ghil, M., Allen, M. R., Dettinger, M. D., Ide, K., Kondrashov, D., Mann, M. E., Robertson, A. W., Saunders, A., tian, Y., & Yiou, P., 2002, Advanced spectral methods for climatic time series. Rev. Geophys.40, 1003.

Griffith, D. , 2008, Spatial-filtering-based contributions to a critique of geographically weighted regression (GWR). *Environment and Planning A* 40(11), 2751-2769.

Guilyardi, E., Wittenberg, A. Fedorov, A., Collins, M., Wang, C., Capotondi, A., Oldenborgh, G., & Stockdale, T., 2009, Atmosphere feedbacks during ENSO in a coupled GCM with a modified atmospheric convection scheme. *J. Climate* **22**, 5698–5718 (2009)

Houborg, R., Soegaard, H., and Boegh, E. ,2007, Combining vegetation index and model inversion methods for the extraction of key vegetation biophysical parameters using Terra and Aqua MODIS reflectance data. Remote Sensing of Environment, 106, 39−58.

Huete, A.R., and Jackson, R.D., 1988,. Soil and atmosphere influences on the spectra of partial canopies, Remote Sensing of the Environment 25:89-105.

Heute A, Didan K, Miura T, Rodriguez EP, Gao X, Ferreira LG., 2002, Overview of the radiometric performance of the MODIS vegetation indices. Remote Sensing Environ. 2002;83:195–213.

Janicot S, Mounier F, Hall NMJ, Leroux S, Sultan B, & Kiladis G.N., 2009, The West African Monsoon dynamics. Part IV: Analysis of the 25–90 day variability of convection and the role of the Indian monsoon. *J. Climate* **22**: 1541–1565.

Janowiak, J. ,1988, An investigation of Interannual Rainfall Variability in Africa. J. Climate, 1, 240-255.

Jiang, Z., Huete, A.R., Didan, K., & Miura, T., 2008, Development of a two-band enhanced vegetation index without a blue band. Remote Sensing of Environment 112, 3833–3845.

Karnauskas, Kristopher B. & Antonio J. Busalacchi, 2009, The role of SST in the East Pacific Warm Pool in the interannual variability of central American rainfall, Journal of climate V.22, 2009

Li, J., Lewis, J., Rowland, J., Tappan,G., Tieszen, L.L. , 2004, Evaluation of land performance in Senegal using multi-temporal NDVI and rainfall series, Journal of Arid Environments, 59 (2004), pp. 463 – 480

Lillesand, T.M. & Kiefer, R.W., 2006. Remote Sensing and Image Interpretation, 6th ed. Wiley, New York, NY.

Martiny, N., Y. Richard, and Camberlin, P., 2005, Interannual persistence effects in vegetation dynamics of semi-arid Africa, Geographical Research Letters, VOL. 32, L24403, 2005

Martiny, N. , Camberlin, P. , Richard, Y. and Philippon, N., 2006, Compared regimes of NDVI and rainfall in semi-arid regions of Africa, International Journal of Remote Sensing, 27: 23, 5201 — 5223

Martiny, N., Philippon, N., Richard, Y., Camberlin, P., & Reason, C., 2010, Predictability of NDVI in semi-arid African regions, Theoretical and applied climatology, 100:467-484

NASA, 2012, MODIS web, http://modis.gsfc.nasa.gov/about/specifications.php, last accessed May 19th., 2012

Nicholson, S.E., 1996. A review of climate dynamics and climate variability in eastern Africa. In: Johnson, T.C., Odada, E., Eds., pp. 25–56 in *The Limnology, Climatology and Paleoclimatology of the East African Lakes*. Gordon & Breach.

Nicholson, S.E., 2000, The nature of rainfall variability over Africa on time scales of decades to millenia, Global and Planetary Change 26 , 2000. 137–158

Nicholson, S.E., Davenport, M. L. and Malo, A, R., 1990, A comparison of the vegetation response to rainfall in the Sahel and East Africa, Using Normalized Difference Vegetation Index From NOAA AVHRR, Climate change Dec. 1990

Nippert, J. B., T. W. Ocheltree, A. M. Skibbe, L. C. Kangas, J. M. Ham, K. B. Shonkwiler Arnold, & Brunsell, N. A., 2011, Linking plant growth responses across topographic gradients in tallgrass prairie. Oecologia.

NREL, 2011, Natural Resource Ecology Laboratory, Colorado State University, viewed Oct. 2011 < http://www.nrel.colostate.edu/ftp/coughenour/ >

O'Sullivan, D., & Unwin, D. ,2010, *Geographic information analysis*. Wiley, Hoboken.

Pohl B, Janicot S, Fontaine B, & Marteau R., 2009, Implication of the Madden–Julian Oscillation in the 40-day variability of the West African Monsoon. J Clim 22:3769–3785

Propastin, P. & Kappas, M. ,2008, Spatiotemporal drifts in AVHRR/NDVI-precipitation relationship and their linkage to Land Use Change in Central Kazakhstan. EARSEL eProceedings, Vol. 7, Issue 1: 30-45.

Propastin, P. ,2012, Modifying geographically weighted regression for estimating aboveground biomass in tropical rainforests by multispectral remote sensing data. International Journal of Applied Earth Observation and Geoinformation, Volume 18, August 2012, Pages 82-90.

Richard, Y., & Poccard, I., 1998, a statistical study of NDVI sensitivity to seasonal and interannual rainfall variations in Southern Africa. International Journal of Remote Sensing, 19, 2907-2920.

Ropelewski, C.F. & Halpert, M.S., 1987, Global and regional scale precipitation patterns associated with El Niño/Southern Oscillation, Mon. Wea. Rev. 115:1606-1626.

Ropelewski, C.F. & M.S. Halpert, 1989. Precipitation patterns associated with high index phase of Southern Oscillation, J. Climate, 2:268-284.

Ropelewski, C. F., & M Halpert,. S., 1996, Quantifying Southern Oscillation–precipitation relationships. J. Climate,9, 1043–1059.

Rouse, J.W., Hass, R.H., Shcell, J.A., & Deering, D.W., 1973, Monitoring vegetation system in the Great Plains with ERTS. In 3rd ERTS synmposium, NASA SP- 351 I, pp. 309-317

Saji, N. H., Goswami, B. N. , Vinayachandran, P. N. & Yamagata, T., 1999, A dipole mode in the tropical Indian Ocean. Nature, 401, 360–363.

Saji N.H. & Yamagata, T., 2003, Possible impacts of Indian Ocean Dipole mode events on global climate. Climate Research, Vol. 25: 151-169, 2003

Scanlon, T. M., J. D. Albertson, K. K. Caylor, and C. A. Williams. 2002. Determining land surface fractional cover from NDVI and rainfall time series for a savanna ecosystem. Remote Sensing of Environment 82:376-388.

Shinoda, M., 1995, Seasonal phase lag between rainfall and vegetation activity in tropical Africa as revealed by NOAA satellite data, International Journal of Climatology, 15 (1995), pp. 639 – 656

Shisanya, C. A., Recha, C., Anyamba,A., 2011, Rainfall Variability and Its Impact on Normalized Difference Vegetation Index in Arid and Semi-Arid Lands of Kenya, International Journal of Geosciences, 2011, 2, 36-47
Thornton, P.E., Running, S.W., White, M.A., & Razuvaev, V., 1997, Generating surfaces of daily meteorology variables over large regions of complex terrain, Journal of Hydrology 190: 214-251

Sinclair A.R.E., 1995, *Serengeti II: Dynamics, Management, and Conservation of an Ecosystem*, University of Chicago Press

Sjostrom, M, Ardo, J. , Arneth, A., Boulain, N., Cappelaere, B., Eklundh, L., de Grandcourt, A., Kutsch, W.L. , Merbold, L. , Nouvellon,Y., Scholes, R.J., Schubert,P., Seaquist, J., & Veenendaal, E.M., 2011, Exploring the potential of MODIS EVI for modeling gross primary production across African ecosystems, Remote Sensing of Environment, Volume 115, Issue 4, 15 April 2011, Pages 1081-1089.

Solano, R., Didan, K., Jacobson, A. & Huete, A., 2010, MODIS vegetation index user's guide (MOD13 series) version 2.00 (collection 5). The University of Arizona, http://vip.arizona.edu, last accessed July 20th. 2012

Tobler, W. 2004. On the first law of geography: A reply. Annals of the Association of American Geographers, 94(2), 304–310.

The Pennsylvania State University, viewed Oct. 2011, <http://www.courses.psu.edu/test/test100_hkr/AFIM/Body_HTML/ITCZ.html>

Thornton, P. E., S. W. Running, & M. A. White, 1997, Generating surfaces of daily meteorological variables over large regions of complex terrain. J. Hydrol.,190, 214–251.

University of South Carolina, viewed Oct. 2011
<http://people.cas.sc.edu/carbone/modules/mods4car/africa-itcz/index.html>

Wang, J, P.M. Rich, and K.P. Price, 2003, Temporal responses of NDVI to precipitation and temperature in the central Great Plains, USA, INT. J. Remote Sensing ,2003, Vol. 24, No. 11, 2345-2364

Wang, Q., Ni, J. & Tenhunen, J. ,2005, Application of a geographically-weighted regression analysis to estimate net primary production of Chinese forest ecosystems. Global Ecology and Biogeography, 14: 379–393.

Wheeler, D. C. ,2006, Diagnostic tools and a remedial method for collinearity in geographically weighted regression. *Environment & Planning A* 39(10), 2464-2481.

Wheeler, D, & Calder C. ,2007, An assessment of coefficient accuracy in linear regression models with spatially varying coefficients. *Journal of Geographical Systems* **9**(2) 145 – 166

Wheeler, D. & Tiefelsdorf, M. ,2005, Multicollinearity and correlation among local regression coefficients in geographically weighted regression. *Journal of Geographical Systems,* **7**, 161–187.

Wilks, Daniel S., 1995, Statistical methods in the atmospheric science

Xiao, X., Hollinger, D., Aber, J., Goltz, M., Davidson, E. A., Zhang, Q., et al., 2004, Satellite based modeling of gross primary production in an evergreen needle leaf forest. Remote Sensing of Environment, 89, 519−534.

Tucker, Sally S., Joseph M. Craine, & Jesse B. Nippert. ,2011, Physiological drought tolerance and the structuring of tallgrass prairie assemblages. Ecosphere 2:art48

Yiou, P., Baert, E., Loutre, M. F., 1996, Spectral analysis of climate data, Surveys in Geophysics vol.17 issue 6, P619 - 663

Zhao, M., Heinsch, F. A., Nemani, R. R., & Running, S. (2005). Improvements of the MODIS terrestrial gross and net primary production global data set. Remote Sensing of Environment, 95, 164−176.

Zhao N, Yang Y, & Zhou X. ,2010, Application of geographically weighted regression in estimating the effect of climate and site conditions on vegetation distribution in Haihe Catchment, China. Plant Ecol 209:349–359.

## Appendix: required permissions for using images

**ELSEVIER LICENSE**
TERMS AND CONDITIONS
Jul 26, 2012

---

---

This is a License Agreement between junyan ding ("You") and Elsevier ("Elsevier") provided by Copyright Clearance Center ("CCC"). The license consists of your order details, the terms and conditions provided by Elsevier, and the payment terms and conditions.

**All payments must be made in full to CCC. For payment instructions, please see information listed at the bottom of this form.**

| | |
|---|---|
| Supplier | Elsevier Limited<br>The Boulevard,Langford Lane<br>Kidlington,Oxford,OX5 1GB,UK |
| Registered Company Number | 1982084 |
| Customer name | junyan ding |
| Customer address | BR 215A, 3226 24th Ave NW<br>Calgary, AB T2N4V3 |
| License number | 2956801161942 |
| License date | Jul 26, 2012 |
| Licensed content publisher | Elsevier |
| Licensed content publication | Global and Planetary Change |
| Licensed content title | The nature of rainfall variability over Africa on time scales of decades to millenia |
| Licensed content author | Sharon E Nicholson |
| Licensed content date | November 2000 |
| Licensed content volume number | 26 |
| Licensed content issue number | 1–3 |
| Number of pages | 22 |
| Start Page | 137 |
| End Page | 158 |
| Type of Use | reuse in a thesis/dissertation |
| Portion | figures/tables/illustrations |
| Number of figures/tables/illustrations | 3 |
| Format | electronic |
| Are you the author of this Elsevier | No |

article?

| | |
|---|---|
| Will you be translating? | No |
| Order reference number | |
| Title of your thesis/dissertation | Exploring the relationship between monthly precipitation and EVI vegetation productivity index of Serengeti National Park |
| Expected completion date | Aug 2012 |
| Estimated size (number of pages) | 80 |
| Elsevier VAT number | GB 494 6272 12 |
| Permissions price | 0.00 USD |
| VAT/Local Sales Tax | 0.0 USD / 0.0 GBP |
| Total | 0.00 USD |
| Terms and Conditions | |

**INTRODUCTION**

1. The publisher for this copyrighted material is Elsevier. By clicking "accept" in connection with completing this licensing transaction, you agree that the following terms and conditions apply to this transaction (along with the Billing and Payment terms and conditions established by Copyright Clearance Center, Inc. ("CCC"), at the time that you opened your Rightslink account and that are available at any time at http://myaccount.copyright.com).

**GENERAL TERMS**

2. Elsevier hereby grants you permission to reproduce the aforementioned material subject to the terms and conditions indicated.

3. Acknowledgement: If any part of the material to be used (for example, figures) has appeared in our publication with credit or acknowledgement to another source, permission must also be sought from that source. If such permission is not obtained then that material may not be included in your publication/copies. Suitable acknowledgement to the source must be made, either as a footnote or in a reference list at the end of your publication, as follows:

"Reprinted from Publication title, Vol /edition number, Author(s), Title of article / title of chapter, Pages No., Copyright (Year), with permission from Elsevier [OR APPLICABLE SOCIETY COPYRIGHT OWNER]." Also Lancet special credit - "Reprinted from The Lancet, Vol. number, Author(s), Title of article, Pages No., Copyright (Year), with permission from Elsevier."

4. Reproduction of this material is confined to the purpose and/or media for which permission is hereby given.

5. Altering/Modifying Material: Not Permitted. However figures and illustrations may

be altered/adapted minimally to serve your work. Any other abbreviations, additions, deletions and/or any other alterations shall be made only with prior written authorization of Elsevier Ltd. (Please contact Elsevier at permissions@elsevier.com)

6. If the permission fee for the requested use of our material is waived in this instance, please be advised that your future requests for Elsevier materials may attract a fee.

7. Reservation of Rights: Publisher reserves all rights not specifically granted in the combination of (i) the license details provided by you and accepted in the course of this licensing transaction, (ii) these terms and conditions and (iii) CCC's Billing and Payment terms and conditions.

8. License Contingent Upon Payment: While you may exercise the rights licensed immediately upon issuance of the license at the end of the licensing process for the transaction, provided that you have disclosed complete and accurate details of your proposed use, no license is finally effective unless and until full payment is received from you (either by publisher or by CCC) as provided in CCC's Billing and Payment terms and conditions. If full payment is not received on a timely basis, then any license preliminarily granted shall be deemed automatically revoked and shall be void as if never granted. Further, in the event that you breach any of these terms and conditions or any of CCC's Billing and Payment terms and conditions, the license is automatically revoked and shall be void as if never granted. Use of materials as described in a revoked license, as well as any use of the materials beyond the scope of an unrevoked license, may constitute copyright infringement and publisher reserves the right to take any and all action to protect its copyright in the materials.

9. Warranties: Publisher makes no representations or warranties with respect to the licensed material.

10. Indemnity: You hereby indemnify and agree to hold harmless publisher and CCC, and their respective officers, directors, employees and agents, from and against any and all claims arising out of your use of the licensed material other than as specifically authorized pursuant to this license.

11. No Transfer of License: This license is personal to you and may not be sublicensed, assigned, or transferred by you to any other person without publisher's written permission.

12. No Amendment Except in Writing: This license may not be amended except in a writing signed by both parties (or, in the case of publisher, by CCC on publisher's behalf).

13. Objection to Contrary Terms: Publisher hereby objects to any terms contained in any purchase order, acknowledgment, check endorsement or other writing prepared by you, which terms are inconsistent with these terms and conditions or CCC's Billing and Payment terms and conditions. These terms and conditions, together with CCC's Billing and Payment terms and conditions (which are incorporated herein), comprise the entire

agreement between you and publisher (and CCC) concerning this licensing transaction. In the event of any conflict between your obligations established by these terms and conditions and those established by CCC's Billing and Payment terms and conditions, these terms and conditions shall control.

14. Revocation: Elsevier or Copyright Clearance Center may deny the permissions described in this License at their sole discretion, for any reason or no reason, with a full refund payable to you. Notice of such denial will be made using the contact information provided by you. Failure to receive such notice will not alter or invalidate the denial. In no event will Elsevier or Copyright Clearance Center be responsible or liable for any costs, expenses or damage incurred by you as a result of a denial of your permission request, other than a refund of the amount(s) paid by you to Elsevier and/or Copyright Clearance Center for denied permissions.

**LIMITED LICENSE**

The following terms and conditions apply only to specific license types:

15. **Translation**: This permission is granted for non-exclusive world **English** rights only unless your license was granted for translation rights. If you licensed translation rights you may only translate this content into the languages you requested. A professional translator must perform all translations and reproduce the content word for word preserving the integrity of the article. If this license is to re-use 1 or 2 figures then permission is granted for non-exclusive world rights in all languages.

16. **Website**: The following terms and conditions apply to electronic reserve and author websites:
**Electronic reserve**: If licensed material is to be posted to website, the web site is to be password-protected and made available only to bona fide students registered on a relevant course if:
This license was made in connection with a course,
This permission is granted for 1 year only. You may obtain a license for future website posting,
All content posted to the web site must maintain the copyright information line on the bottom of each image,
A hyper-text must be included to the Homepage of the journal from which you are licensing at http://www.sciencedirect.com/science/journal/xxxxx or the Elsevier homepage for books at http://www.elsevier.com , and
Central Storage: This license does not include permission for a scanned version of the material to be stored in a central repository such as that provided by Heron/XanEdu.

17. **Author website** for journals with the following additional clauses:

All content posted to the web site must maintain the copyright information line on the bottom of each image, and the permission granted is limited to the personal version of your paper. You are not allowed to download and post the published electronic version of your

article (whether PDF or HTML, proof or final version), nor may you scan the printed edition to create an electronic version. A hyper-text must be included to the Homepage of the journal from which you are licensing at http://www.sciencedirect.com/science/journal/xxxxx . As part of our normal production process, you will receive an e-mail notice when your article appears on Elsevier's online service ScienceDirect (www.sciencedirect.com). That e-mail will include the article's Digital Object Identifier (DOI). This number provides the electronic link to the published article and should be included in the posting of your personal version. We ask that you wait until you receive this e-mail and have the DOI to do any posting.

Central Storage: This license does not include permission for a scanned version of the material to be stored in a central repository such as that provided by Heron/XanEdu.

18. **Author website** for books with the following additional clauses:
Authors are permitted to place a brief summary of their work online only.
A hyper-text must be included to the Elsevier homepage at http://www.elsevier.com . All content posted to the web site must maintain the copyright information line on the bottom of each image. You are not allowed to download and post the published electronic version of your chapter, nor may you scan the printed edition to create an electronic version.

Central Storage: This license does not include permission for a scanned version of the material to be stored in a central repository such as that provided by Heron/XanEdu.

19. **Website** (regular and for author): A hyper-text must be included to the Homepage of the journal from which you are licensing at http://www.sciencedirect.com/science/journal/xxxxx. or for books to the Elsevier homepage at http://www.elsevier.com

20. **Thesis/Dissertation**: If your license is for use in a thesis/dissertation your thesis may be submitted to your institution in either print or electronic form. Should your thesis be published commercially, please reapply for permission. These requirements include permission for the Library and Archives of Canada to supply single copies, on demand, of the complete thesis and include permission for UMI to supply single copies, on demand, of the complete thesis. Should your thesis be published commercially, please reapply for permission.

21. **Other Conditions**:

v1.6

**If you would like to pay for this license now, please remit this license along with your payment made payable to "COPYRIGHT CLEARANCE CENTER" otherwise you will be invoiced within 48 hours of the license date. Payment should be in the form of a check or money order referencing your account number and this invoice number RLNK500826575.**

**Once you receive your invoice for this order, you may pay your invoice by credit card. Please follow instructions provided at that time.**

**Make Payment To:**
**Copyright Clearance Center**
**Dept 001**
**P.O. Box 843006**
**Boston, MA 02284-3006**

**For suggestions or comments regarding this order, contact RightsLink Customer Support: customercare@copyright.com or +1-877-622-5543 (toll free in the US) or +1-978-646-2777.**

**Gratis licenses (referencing $0 in the Total field) are free. Please retain this printable license for your reference. No payment is required.**

**SPRINGER LICENSE**
**TERMS AND CONDITIONS**

Jul 27, 2012

This is a License Agreement between junyan ding ("You") and Springer ("Springer") provided by Copyright Clearance Center ("CCC"). The license consists of your order details, the terms and conditions provided by Springer, and the payment terms and conditions.

**All payments must be made in full to CCC. For payment instructions, please see information listed at the bottom of this form.**

| | |
|---|---|
| License Number | 2956870979765 |
| License date | Jul 27, 2012 |
| Licensed content publisher | Springer |
| Licensed content publication | Springer eBook |
| Licensed content title | Introduction To Spectral Analysis |
| Licensed content author | |
| Licensed content date | Mar 6, 2008 |
| Type of Use | Thesis/Dissertation |
| Portion | Figures |
| Author of this Springer article | No |
| Order reference number | |
| Title of your thesis / dissertation | Exploring the relationship between monthly precipitation and EVI vegetation productivity index of Serengeti National Park |
| Expected completion date | Aug 2012 |
| Estimated size(pages) | 80 |
| Total | 0.00 USD |
| Terms and Conditions | |

Introduction

The publisher for this copyrighted material is Springer Science + Business Media. By clicking "accept" in connection with completing this licensing transaction, you agree that the following terms and conditions apply to this transaction (along with the Billing and Payment terms and conditions established by Copyright Clearance Center, Inc. ("CCC"), at the time that you opened your Rightslink account and that are available at any time at

http://myaccount.copyright.com).

Limited License

With reference to your request to reprint in your thesis material on which Springer Science and Business Media control the copyright, permission is granted, free of charge, for the use indicated in your enquiry.

Licenses are for one-time use only with a maximum distribution equal to the number that you identified in the licensing process.

This License includes use in an electronic form, provided its password protected or on the university's intranet or repository, including UMI (according to the definition at the Sherpa website: http://www.sherpa.ac.uk/romeo/). For any other electronic use, please contact Springer at (permissions.dordrecht@springer.com or permissions.heidelberg@springer.com).

The material can only be used for the purpose of defending your thesis, and with a maximum of 100 extra copies in paper.

Although Springer holds copyright to the material and is entitled to negotiate on rights, this license is only valid, provided permission is also obtained from the (co) author (address is given with the article/chapter) and provided it concerns original material which does not carry references to other sources (if material in question appears with credit to another source, authorization from that source is required as well).

Permission free of charge on this occasion does not prejudice any rights we might have to charge for reproduction of our copyrighted material in the future.

Altering/Modifying Material: Not Permitted

You may not alter or modify the material in any manner. Abbreviations, additions, deletions and/or any other alterations shall be made only with prior written authorization of the author(s) and/or Springer Science + Business Media. (Please contact Springer at (permissions.dordrecht@springer.com or permissions.heidelberg@springer.com)

Reservation of Rights

Springer Science + Business Media reserves all rights not specifically granted in the combination of (i) the license details provided by you and accepted in the course of this licensing transaction, (ii) these terms and conditions and (iii) CCC's Billing and Payment terms and conditions.

Copyright Notice:Disclaimer

You must include the following copyright and permission notice in connection with any reproduction of the licensed material: "Springer and the original publisher /journal title, volume, year of publication, page, chapter/article title, name(s) of author(s), figure number(s), original copyright notice) is given to the publication in which the material was originally published, by adding; with kind permission from Springer Science and Business

Media"

Warranties: None

Example 1: Springer Science + Business Media makes no representations or warranties with respect to the licensed material.

Example 2: Springer Science + Business Media makes no representations or warranties with respect to the licensed material and adopts on its own behalf the limitations and disclaimers established by CCC on its behalf in its Billing and Payment terms and conditions for this licensing transaction.

Indemnity
You hereby indemnify and agree to hold harmless Springer Science + Business Media and CCC, and their respective officers, directors, employees and agents, from and against any and all claims arising out of your use of the licensed material other than as specifically authorized pursuant to this license.

No Transfer of License
This license is personal to you and may not be sublicensed, assigned, or transferred by you to any other person without Springer Science + Business Media's written permission.

No Amendment Except in Writing
This license may not be amended except in a writing signed by both parties (or, in the case of Springer Science + Business Media, by CCC on Springer Science + Business Media's behalf).

Objection to Contrary Terms
Springer Science + Business Media hereby objects to any terms contained in any purchase order, acknowledgment, check endorsement or other writing prepared by you, which terms are inconsistent with these terms and conditions or CCC's Billing and Payment terms and conditions. These terms and conditions, together with CCC's Billing and Payment terms and conditions (which are incorporated herein), comprise the entire agreement between you and Springer Science + Business Media (and CCC) concerning this licensing transaction. In the event of any conflict between your obligations established by these terms and conditions and those established by CCC's Billing and Payment terms and conditions, these terms and conditions shall control.

Jurisdiction
All disputes that may arise in connection with this present License, or the breach thereof, shall be settled exclusively by arbitration, to be held in The Netherlands, in accordance with Dutch law, and to be conducted under the Rules of the 'Netherlands Arbitrage Instituut' (Netherlands Institute of Arbitration).***OR:***

**All disputes that may arise in connection with this present License, or the breach thereof, shall be settled exclusively by arbitration, to be held in the Federal Republic**

**of Germany, in accordance with German law.**

**Other terms and conditions:**

**v1.3**

**If you would like to pay for this license now, please remit this license along with your payment made payable to "COPYRIGHT CLEARANCE CENTER" otherwise you will be invoiced within 48 hours of the license date. Payment should be in the form of a check or money order referencing your account number and this invoice number RLNK500826616.**
**Once you receive your invoice for this order, you may pay your invoice by credit card. Please follow instructions provided at that time.**

**Make Payment To:**
**Copyright Clearance Center**
**Dept 001**
**P.O. Box 843006**
**Boston, MA 02284-3006**

**For suggestions or comments regarding this order, contact RightsLink Customer Support: customercare@copyright.com or +1-877-622-5543 (toll free in the US) or +1-978-646-2777.**

**Gratis licenses (referencing $0 in the Total field) are free. Please retain this printable license for your reference. No payment is required.**